NOVA SCHOOL OF SCIENCE & TECHNOLOGY

DEPARTMENT OF PHYSICS

MARIANA GARCÊS MEIRA ROXO

Licenciate in Sciences of Biomedical Engineering

EOG/EEG ACQUISITION AND ANALYSIS FOR DISCRIMINATION OF TYPICAL RESPONSES IN THE HIGH PASS BAND

MASTER IN BIOMEDICAL ENGINEERING

NOVA University Lisbon
March, 2023

NOVA SCHOOL OF SCIENCE & TECHNOLOGY

DEPARTMENT OF PHYSICS

EOG/EEG ACQUISITION AND ANALYSIS FOR DISCRIMINATION OF TYPICAL RESPONSES IN THE HIGH PASS BAND

MARIANA GARCÊS MEIRA ROXO

Licenciate in Sciences of Biomedical Engineering

Adviser: Raul Rato
Assistant Professor, NOVA University Lisbon

Examination Committee

Chair: Doutor Ricardo Nuno Pereira Verga e Afonso Vigário
Associate Professor, NOVA School of Science and Technology

Rapporteur: Doutor Arnaldo Guimarães Baptista
Assistant Professor, NOVA School of Science and Technology

Adviser: Doutor Raul Eduardo Capela Tello Rato
Assistant Professor, NOVA School of Science and Technology

MASTER IN BIOMEDICAL ENGINEERING

NOVA University Lisbon
March, 2023

EOG/EEG ACQUISITION AND ANALYSIS FOR DISCRIMINATION OF TYPICAL RESPONSES IN THE HIGH PASS BAND

Copyright © Mariana Garcês Meira Roxo, NOVA School of Science and Technology, NOVA University Lisbon.

The NOVA School of Science and Technology and the NOVA University Lisbon have the right, perpetual and without geographical boundaries, to file and publish this dissertation through printed copies reproduced on paper or on digital form, or by any other means known or that may be invented, and to disseminate through scientific repositories and admit its copying and distribution for non-commercial, educational or research purposes, as long as credit is given to the author and editor.

This document was created with the (pdf/Xe/Lua)LaTeX processor and the NOVAthesis template (v6.9.4) [1].

Acknowledgements

It is with a lot of mixed feelings that I write these acknowledgments. On one hand, I am so grateful to watch the culmination of this very challenging but also very rewarding degree. They were almost 5 years that truly felt like a decade. In the beginning, I felt very clueless about what I had just chosen to be the trajectory for my next 5 years. I was just trying to find the best way of postponing my entrance into unemployment, to be completely honest. Then, when I finally felt comfortable, a global pandemic (a "pandumia", if you will, in the words of the wise Jorge Jesus) started which made us all adjust to a new reality. The worst thing about this was not only not being able to be with anybody and being confined to 4 walls, but especially having to say goodbye to the routine of having lunch on the lawn of the NOVA School of Science and Technology's library, talking in the sun and relaxing, recharging batteries and our mental sanity, that this degree kept testing over and over again.

It was hard but it would have been even harder if it hadn't been for the very empowering and best group of female engineers, "Repolariza-te, miúda", that will surely revolutionize Science all across the globe. I especially want to thank my Joanas, Joana Coutinho and Joana Santos, for always being there for me whenever I need them the most. The only thing I would change about you both would be your addresses because we truly have a long-distance relationship with each other. I wanna thank Pedro, that is (almost) always there for me to hear my deepest fears and frustrations even though he really does not understand most of what I say regarding my degree, as what happens with my family. I want to thank my mom, who always supported me and believed in me even when I was not able to do it myself. For teaching me to work for myself and always wanting more, even when it seems like all the odds are against us. I want to thank my brother and my aunt for teaching me to believe I am worthy of every opportunity just like everybody else and for feeding me delicious food to fuel my brain, respectively. I want to thank my dad for insisting that math is fun. It is not just fun. It is fun-tastic (I am so very sorry for that pun). I also want to thank my adviser, Raul Rato, for being so patient with me, for valuing my work and for the availability he showed in helping me accomplish this work. I want to thank my experimental subjects, Ricardo and Tomás in particular, that traveled all the way from Lisbon to sunny Caparica to be my lab rats without hesitation because only God knows how hard it is to find people that do not object to putting gel in their scalps and crossing the 25th of April Bridge all in the name of Science.

I am so so thrilled to be called a master in Biomedical Engineering and I can not wait to stop working for free.

"The beautiful thing about learning is that nobody can take it away from you." (B.B. King)

ABSTRACT

The link between saccadic movements and neurological diseases has proven to be interesting, since the former change as a result of the latter. These diseases are often challenging to diagnose, as they may already be at an extremely developed stage at the time of diagnosis.

In this thesis, these movements were used in order to develop a model of the transmission of information in the brain, aiming at investigating typical response patterns in detection of the transmitted information.

For this purpose, 6 subjects were presented with a slide show, designed using a 127 m-sequence, as to avoid any learning phenomenon. During the experiment, electroencephalography (EEG) and electrooculography (EOG) signals were collected. An algorithm was then developed whose goal was to estimate the previously presented sequence using only the signals collected above certain frequencies. Subsequently, typical responses in detection were analyzed.

For all subjects, only one sequence was correctly detected, namely the one that had been selected to be shown. With increasing cutoff frequency, the number of detections tended to increase. At lower cutoff frequencies, the number of detections was substantially lower for one of the subjects. For three subjects, rates of 100% were reached, which were considered abnormal.

In summary, the algorithm proved to be efficient in estimating the sequences using the EEG and EOG signals as objects of analysis. In the future, if the algorithm is tested on subjects with pathology, it is proposed that healthy subjects will show non-pathological patterns and unhealthy subjects will show patterns of pathological ones. If this hypothesis is confirmed, this algorithm could contribute to a potential predictor of a biomarker for these diseases in the future.

Keywords: EEG, EOG, m-sequences, matched filter, saccades

The research work described in this dissertation was carried out in accordance with the norms established in the ethics code of Universidade Nova de Lisboa. The work described and the material presented in this dissertation, with the exceptions clearly indicated, constitute original work carried out by the author.

RESUMO

O elo de ligação entre os movimentos sacádicos e as doenças neurológicas tem demonstrado interesse, uma vez que os primeiros sofrem alterações em consequência das segundas. Estas doenças são muitas vezes difíceis de diagnosticar, uma vez que podem já estar numa fase extremamente desenvolvida aquando do diagnóstico.

Nesta tese, estes movimentos foram utilizados para modelar a transmissão de informação no cérebro, com vista a investigar padrões de resposta típicos na deteção da informação transmitida.

Para o efeito, foi apresentada a 6 indivíduos uma apresentação de diapositivos, concebida a partir de uma m-sequência de 127 bits para evitar qualquer fenómeno de aprendizagem. Durante a experiência, foram recolhidos sinais EEG e EOG. Foi então desenvolvido um algoritmo cujo objetivo era estimar a sequência previamente apresentada utilizando apenas os sinais recolhidos acima de determinadas frequências. Posteriormente, foram analisadas as respostas típicas na deteção.

Para todos os sujeitos, apenas uma sequência foi corretamente detectada, nomeadamente a que foi selecionada para ser apresentada. Com o aumento da frequência de corte, mais canais tenderam a estimar corretamente a sequência. Em frequências de corte mais baixas, a taxa de sucesso foi substancialmente menor para um dos sujeitos. Para três sujeitos, foram atingidas taxas de 100%, consideradas anómalas.

Em resumo, o algoritmo mostrou-se eficiente na estimativa das sequências utilizando os sinais EEG e EOG como objectos de análise. No futuro, se o algoritmo for testado em sujeitos com patologia, propõe-se que sujeitos saudáveis apresentem padrões não patológicos e sujeitos não saudáveis apresentem padrões patológicos. Se esta hipótese for confirmada, este algoritmo poderá contribuir para um potencial precedente de um biomarcador para estas doenças no futuro.

Palavras-chave: EEG, EOG, m-sequências, filtro adaptado, movimentos sacádicos

O trabalho de investigação descrito nesta dissertação foi realizado de acordo com as normas estabelecidas no código de ética da Universidade Nova de Lisboa. O trabalho descrito e o material apresentado nesta dissertação, com as exceções claramente indicadas, constituem trabalho

original realizado pela autora.

CONTENTS

List of Figures

List of Tables

ACRONYMS

AD	Alzheimer's disease
AS	antisaccade
AWGN	additive white gaussian noise
CMS	common mode sense
CNN	convolution neural networks
CNS	central nervous system
DEE	Department of Electrical and Computer Engineering
DLB	dementia with Lewy bodies
DRL	driven right leg
ECG	electrocardiogram
EEG	electroencephalography
EOG	electrooculography
ERP	event-related potential
FB	frequency breakpoints
FC	Faraday cage
FCT NOVA	NOVA School of Science and Technology
FFT	fast Fourier transform
IST	inverting Schmitt trigger
LFSR	linear feedback shift register
MGS	memory-guided saccade
NRZ	non-return-to-zero
PD	Parkinson's disease

REM rapid eye movement
RZ return-to-zero

SNR signal-to-noise ratio

VGS visually guided saccade
VOR vestibulo-ocular reflex

XOR exclusive OR

SYMBOLS

f	cutoff frequency for the high pass filter
χ	name of the .bdf file corresponding to every acquisition
f_s	sampling frequency
V_{IH}	high level threshold voltage
V_{IL}	low level threshold voltage

CHAPTER 1

INTRODUCTION

1.1 Motivation

Studying the information transmission in the brain can help in understanding how it is impaired in certain neurological diseases, which can further contribute to new biomarkers that can make the diagnosis more accurate and, hopefully, in an earlier stage. One of the main problems in diagnosing these diseases is that the doctor only prescribes tests to confirm the presence of disease after symptoms have been observed. Nevertheless, by the time the diagnosis is confirmed, it may already be too late for the therapy to take effect. Additionally, due to the overlap in symptoms, some diseases can be misdiagnosed, which will have implications for the treatment, which can be dangerous for the patients. It becomes imperative to find new biomarkers that are able to screen these pathologies in an early stage.

With this in mind, the main aim of this dissertation was to obtain a model of the brain regarding its ability to process information, so it can be linked to patterns of pathology that can provide help distinguishing between healthy and unhealthy subjects.

Models' main focus are the way a certain structure works. They require a mathematical quantitative description of the relationship between the stimuli and the measured reactions. In this work, the brain works as "black box"that receives an experimental stimulus (a visual stimuli, in this case), and its response is measured using EEG and EOG. Using the patterns of detection later found, the attempt was to model the transmission of information.

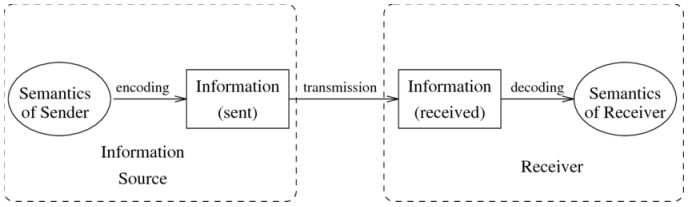

Figure 1.1: Elements of information transmission in [2].

Information transmission can be described as a series of steps shown in figure 1.1. There are two actors as far as the transmission of information is concerned: the information source and the receiver. In the information source lies the sender, which/who intends to send a message to the receiver, and to accomplish that, it must be encoded. After encoding, a transmission means is chosen and, when it reaches the receiver, it must be decoded.

In this study, saccades in response to a visual stimuli were studied. The visual stimuli in question were slides, built from a 127-bit m-sequence. The m-sequence was considered the message to be transmitted to the receiver (the subjects). In order to encode this message, Manchester coding in non-return-to-zero (NRZ) was used, which resulted in a stimulus consisting of 259 slides shown to the subjects. The visual stimuli chosen were slides with circles whose position would vary on the screen, being either on the left or right, stimulating saccades. Visual stimuli have the advantage of being relatively easy to collect since EEG pick up is easy on the visual cortex. They are also easy to manipulate and are free of ethical approval.

As the model must be data-based, the data used were EEG and EOG which have the advantage of being non-intrusive and inexpensive to collect, as opposed to brain imaging techniques. EEG also holds the advantage of having a high temporal resolution, which allows for the study of the cognitive process good temporal precision and understand the underlying brain activity [3]. For instance, when studying epilepsy, it has been proven to be an efficient tool to detect epileptic seizures in conjunction with convolution neural networks (CNN), achieving success rates of 95% without feedback and 97% with feedback [4]. When used to study dementia, it is speculated that changes in EEG can be helpful to discriminate different causes of dementia [5].

As for EOG, these have also been linked to the studies of psychopathologies, especially regarding saccadic eye movements since changes have been noticed when studying these diseases [6]. Eye movements have been shown to be interesting ways to study cognitive impairment, in that they are able to mirror it, making them an interesting object of study in the field of pre-diagnosis [7].

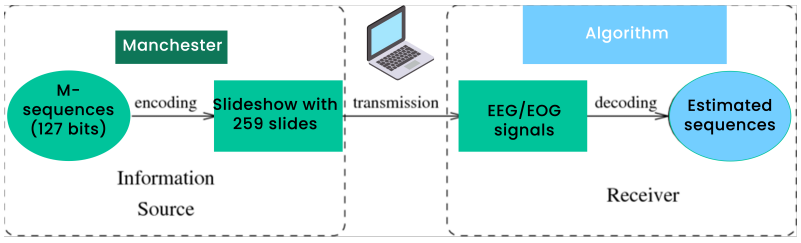

Figure 1.2: Transmission of the information in the framework of the dissertation work based on figure 1.1.

Figure 1.2 sums up the framework used in this work. Using solely the data collected, it was desired to retrieve the sequences previously shown to the subjects by estimating them in every recorded channel using a matched filter. The patterns of estimation serve as the basis for the model and it is expected that healthy subjects will display characteristic patterns of a

healthy individual whereas unhealthy subjects will display other patterns, typical of a patient with pathology. If this hypothesis proves to be successful, this can be the beginning of a new way of diagnosing that does not rely on symptoms and can be used as a screening tool in order to perform earlier and more accurate diagnoses using saccades, analyzed using EEG and EOG, as biomarkers for neurological diseases.

1.2 Objectives

This dissertation aims at developing a model of information processing in the brain, using saccades as the object of study, measured using EEG and EOG. In order to stimulate saccades, visual stimuli were used, built from an m-sequence. The goal was to model the brain by assessing patterns in the retrieval of the sequence to later link them to presence or absence of disease.

Using solely the subjects' EEG and EOG signals above certain frequencies, this sequence should be retrieved using a matched filter as a detection tool.

Considering the time ethics committees can take to authorize studies in patients in hospitals, the development of the algorithm was considered the priority and thus, the experiment was only conducted in healthy subjects. Thus, studying the performance of the algorithm in unhealthy subjects and, consequently, their typical responses were beyond the scope of this dissertation.

However, once these are ascertained, the model can be further developed as far as information transmission goes to assess if the possibility of differentiating between the two groups, using the patterns observed in the detection.

To develop the algorithm, a Data Science Pipeline-approach was chosen.

CHAPTER 2

THEORETICAL BACKGROUND

This section aims to further explain some of the concepts used in this dissertation. An introduction of signals (**EEG** and **EOG**) used to develop the algorithm is done. A section on **saccades** has also been added so that the reader can get a better insight into the experience and how these can be recorded and serve as an object of study. In this dissertation, visual stimuli were used, built from an **m-sequence**. In order to obtain the slideshow presented to the subjects, this m-sequence was encoded using **Manchester encoding** in **NRZ**. In order to store the information of the visual stimuli throughout the acquisition, a circuit was developed. For this circuit, an **inverting Schmitt trigger** was used. Furthermore, a brief explanation of a **binary symmetric channel** was added, as a way of further enlightening the reader on the framework used, more specifically, involved in the information transmission process. The method of detection used was a **matched filter**, which was used to estimate the sequences. In order to determine if the detection had been successful, a criteria based on **Hamming distance** was used, and so, a brief explanation was also included regarding that concept.

2.1 Electroencephalography (EEG)

EEG is the signal obtained by measuring the electrical activity in the brain which results from the additive transmission of multiple nerve impulses by neurons. In this technique, electrodes are put in the scalp (usually using a specific cap) and the data is recorded and then used for diagnostic purposes [8]. It is considered one of the most important methods to assess brain disorders and to monitor the electrical changes in the brain. This technique also has the advantage of having good temporal resolution [9].

It has been mostly used to study epilepsy but it can also be used to study other conditions like dementia, head injury and concussion, brain tumors, encephalitis, and sleep disorders. For instance, EEG waves will be slower in a patient with brain tumor as opposed to a patient

without it.

Because the number of synapses per neuron increases with age but the number of neurons decreases, the number of synapses also decreases over time [8].

There are two types of waves that can be measured in EEG and can be divided according to whether they originated spontaneously (spontaneous rhythms) or in response to an artificial stimulus (evoked potentials).

Spontaneous rhythms usually range from 0.5 to 150 μV in amplitude, and from 0.5 to 60 Hz in frequency [8, 9]. Depending on the latter, they can be classified [8]:

- *delta* (δ): 0.5-4 Hz - Most prominent during the last two stages of sleep [8]. These are usually located in the frontal lobe in adults [9];
- *theta* (θ): 4-8 Hz [8] - Mainly recorded in frontal areas while performing low brain activities, sleep or drowsiness or cognitive processing. Throughout fatigue accumulation and sustained attention, an increase EEG power in this band has been noted, in the frontal, parietal and central regions [9];
- *alpha* (α): 8-13 Hz - Observed better in the posterior and occipital regions, with typical peak-to-peak amplitude $\approx$ 50 μV. This activity is induced by closing the eyes and by relaxation and ceases when they are opened or when some alert mechanism is triggered. These are usually the result of multiple dendrite potentials. In relaxation or sleepiness, the amplitude increases [8];
- *beta* (β): > 13 Hz - Predominate in an awake state and with eyes open [8]. These are recorded in frontal or central areas with the eyes open, being related to consciousness, alertness, arousal, and motor behaviours. Cognitive processes including attention, learning and diverse types of memory usually occur in frequencies higher than 33 Hz [9].

Evoked potentials or event-related potentials, on the other hand, are initiated by an internal or external stimulus [8].

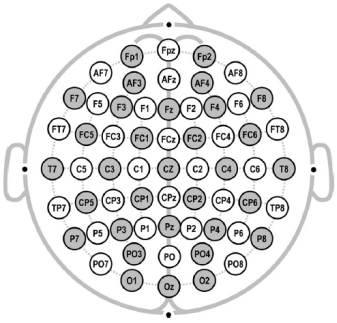

Figure 2.1: International 10-20 system for 32 electrodes (gray circles) [10].

Figure 2.1 shows the standardized electrode positioning for EEG acquisitions when using an electrode cap. Letters stand for the adjacent lobe to the electrode in question.

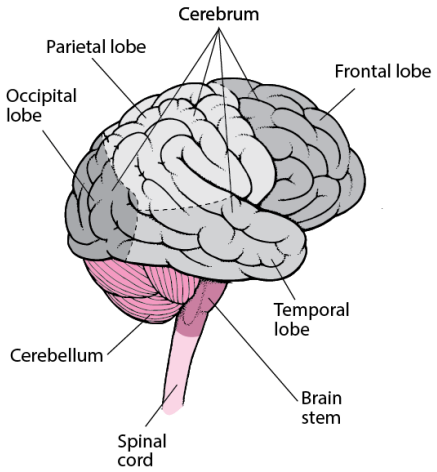

Figure 2.2: Brain lobes [11].

The electrodes' positioning should be chosen according to the activities, and in consequence, to which lobes are being studied. Figure 2.2 shows the four lobes belonging to the cerebrum as well as the rest of the central nervous system (CNS): the cerebellum, the brain stem and the spinal cord.

The four lobes are associated with different functions:

- **frontal lobe** - responsible for planning and executing learned and purposeful tasks. Many inhibitory functions are also located in this lobe;
- **parietal lobe** - integrates stimuli involved in language processing;
- **temporal lobe** - responsible for auditory perception, receptive components of language, visual memory, declarative (factual) memory, and emotion;
- **occipital lobe** - contains the visual primary cortex and the visual association areas.

As far as processing is concerned, wavelet analysis are usually the chosen method for time-frequency analysis. It can also include Fourier transform, Short Time Fourier Transform, Wavelet transform, Hilbert-Hung transform and Empirical Mode Decomposition [9].

2.2 Electrooculography (EOG)

EOG concerns the technique used to measure the resting potential of the retina of human eyes, between the cornea (positive pole) and the back of the eye (retina) (negative pole) [12]. Thus, the eye can be seen as a dipole that rotates during the eye movement and EOG measures that same movement, being usually situated in the range of 0.4-1.0 mV [13]. The electrical potential varies according to the direction of the eyeball movement: it increases if the eyeball moves in the direction of the electrode and decreases if it moves in the opposite direction. The measured potential also depends on the viewing angle, up to an angle of 30º [9, 14].

EOG is commonly used in sleep studies. Similarly to delta and beta waves in EEG, EOG can be used to detect when one is awake or in rapid eye movement (REM) sleep [15].

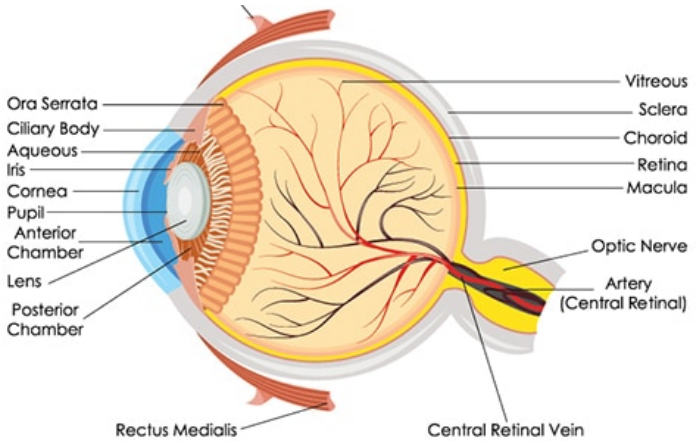

Figure 2.3: Human eye anatomy. [16]

When the light enters the eye, it travels from the cornea to the retina, where there are photosensitive cells, that are sensitive to the incident energy, and neural cells, generating receptor potentials that go from the eye to the brain through the optic nerve.

In the retina, there are rods and cones, that respond to dim light and aid in vision in circumstances where the light is brighter. In these photo receptors, transduction occurs, *i.e.*, the conversion of light in an electric signal that propagates to the visual cortex. Each photo receptor can transduce the energy of a single photon into a current of $\approx$ 1pA that lasts $\approx$ 1 s.

EOG can have two major divisions: saccadic response and nystagmography (the study of small involuntary movements of the eye in response to the moving fluid in the vestibular system) [9, 13].These can be divided essentially into 6 systems of movement: saccadic, smooth pursuit and vergence (with the objective of maintaining the visual target on the fovea) and fixation, vestibulo-ocular reflex (VOR) and optokinetic (whose aim is to keep the eye stable and stationary on a given target [17]).

- **saccades** - Saccades involve all eyes movements that are of relatively high velocity and step-like angular movement of both eyes simultaneously in the same direction [18]. They are relatively easy to spot in EOG because the deflected amplitudes have higher frequencies than the usual noise level and last for shorter periods of time. These movements are responsible for changing the eye direction around the field of view and bringing the object of interest into the fovea. Their duration depends on the angular distance traveled by the eye during the saccade [9]. They are the main fast movements performed by the eye [14];

- **fixations** - Fixations relate to the static state of the eyes when the gaze is held on a fixed point. They can also refer to the movement the eyes perform between two saccades, when the gaze is kept roughly stationary [18]. Their duration can go from 100 to 1000 ms [9];

- **blinks** - Blinks concern the rapid motion performed in order to keep the eyes moist through regular opening and closing of the eyelids [18].

EOG, although having good signal-to-noise ratio (SNR), are very susceptible to artifacts coming from the facial muscles throughout the EOG recording or from EEG, and the spatial resolution is not as good as video-based eye tracking [14]. This technique is considered to be efficient when it comes to detecting drowsiness markers like reduction in performance and alternations in the frequency of the blinking movement [9].

2.3 Saccades

Saccades can reach an angular velocity of up to 500-600º/s. In order to register horizontal saccades, when using EOG, two electrodes are usually placed at both bilateral canthi of the eyes. Saccades can be divided into two main classes:

- externally guided saccades - the ones made in response to an external visual target (involuntarily);
- internally guided saccades - the ones made in the absence of a visual target (voluntarily).

In order to study saccades, three paradigms can be used: visually guided saccade (VGS), memory-guided saccade (MGS) or antisaccade (AS) tasks. In the VGS paradigm, the subjects are instructed to first fixate at the central fixation spot, after which a target appears to the left or right of this fixation point and in the direction of which they are required to make a saccade. In this case, saccades happen in response to a stimulus. When studying internally guided saccades (without a visual stimulus), MGS task is used. Subjects are first instructed to fixate at the central fixation point, similarly to VGS, and then a target appears for a short period of time. Only 1-2 seconds after this target disappears, is the subject meant to make a saccade in the direction of the target, from memory. In AS task, as opposed to VGS, subjects are instructed to look at the target's opposite direction after the central fixation point.

When performing saccade recordings, one of the features is latency, i.e., the time between the target presentation/extinction of the central fixation point and the time a deflection occurs. The amplitude of the saccade is given by the saccade amplitude, and the speed of the saccade by the slope of the deflection. The latency for saccades in VGS is usually 150-200 ms; for MGS, it is usually 200-250 ms.

Internally and externally guided saccades are mediated by different structures, the first one having slightly longer latency and slower peak velocity than the latter.

Saccade abnormality has been registered when studying Parkinson's disease (PD), cerebellar ataxia and progressive supranuclear palsy, which makes it a viable object of study to aid in finding a new biomarker, possibly non-invasive, to screen these and other neurological diseases [14].

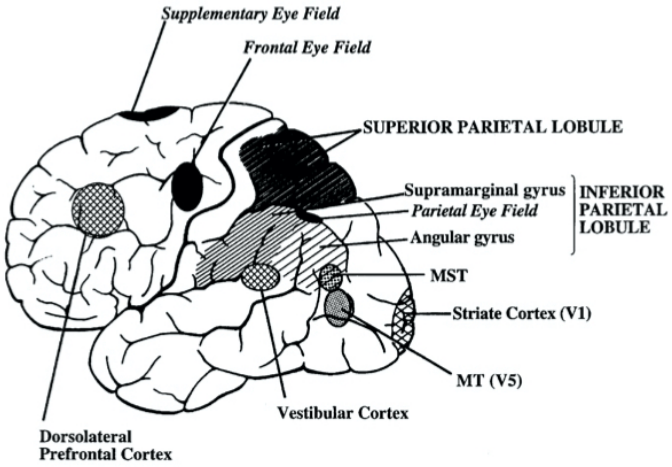

Figure 2.4: Brain structures involved in the generation of saccades [19].

Figure 2.4 shows the main structures involved in producing saccades, some of which are also involved in the changes caused by PD, namely the striatum.

2.4 M-sequences

M-sequence stands for maximum length sequence, referring to the period L, which is the maximum number of iterations in the LFSR until the sequence begins to repeat. They are generated using LFSRs, which follow a rule of linear feedback and recursion [20, 21]. They are binary sequences that require low computational cost to be generated, as the number of computations required and the sequence length are linearly related [22]. Although they seem and, in many ways, behave as completely random [23], they are generated by a kernel (seed), that directly influences the resulting sequence thus, they are said to be pseudorandom noise sequences[20].

Table 2.1: Primitive polynomials up to degree L=9 used to generate m-sequences.

Degree (m)	Sequence length (L)	Primitive polynomial
1	1	$x+1$
2	3	x^2+x+1
3	7	x^3+x+1
4	15	x^4+x+1
5	31	x^5+x^2+1
6	63	x^6+x+1
7	127	x^7+x+1
8	255	$x^8+x^7+x^2+x+1$
9	511	x^9+x^4+1

The length of the LFSR directly influences the length of the resulting sequence, as seen in table 2.1. These sequences are generated infinitely and are periodic, with period L being equal to 2^m-1 when using a LFSR of size m. The generation occurs through a feedback mechanism,

which is why the circuit is called a LFSR. The circuit is controlled using a clock and after each shift, the state of register m switches to the state of register m-1 which was in the previous shift of the clock. The states depend on the operation (based on a mod 2 - adder, which is equivalent to a exclusive OR (XOR) gate) defined for the feedback. The feedback which must be a primitive polynomial in order to generate an m-sequence [23]. In table 2.1, the primitive polynomials are presented in order to generate sequences considering each desired length.

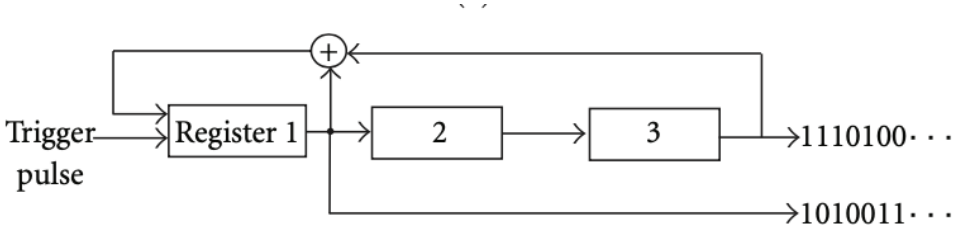

Figure 2.5: 3-stage LFSR (adaptation from [24])

Figure 2.5 is adapted from [24] and shows the circuit that generates an m-sequence with a $m = 3$ stages LFSR, which will result in a sequence with maximum length 7. In this work, m-sequences of length 127 were used as the message to be transmitted, requiring a LFSR with length $m = 7$. The feedback operation is the mod 2 of outputs of register 1 and 3, which correlate to the primitive polynomial presented in table 2.1. The feedback function to generate an m-sequence with L=7 is given by:

$$g(x) = \sum_{k=0}^{L} g_k x^k \quad (mod\ 2) \tag{2.1}$$

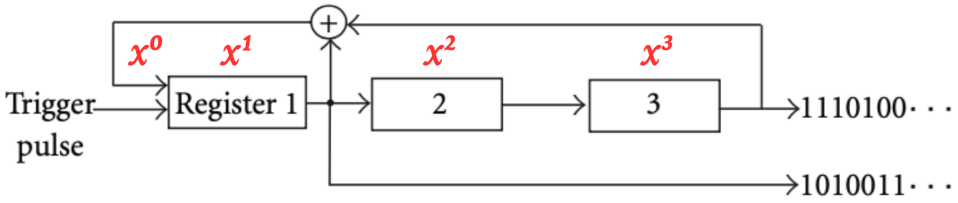

Figure 2.6: Alternative representation of the LFSR in figure 2.5.

Figure 2.5 can be represented by its equivalent in figure 2.6, which will result in the GF(2) polynomials that are used to generate the m-sequences as seen in table 2.1. The serial input (input in Register 1) is obtained by doing the mod 2 of states in registers 1 and 3, *i.e.*, by doing $x^3 + x$. However, if the first state in register 1 is equal to "0", this will result in states "000"over time, which will not result in an m-sequence. In order to overcome that, register 1 must be initialized with "1", which results in a feedback function: $x^3 + x + 1$, as seen in table 2.1, with

$g_0 = 1$ and $g_3 = 1$ when expressing it using equation 2.1. The desired m-sequence will be the register 3's output in this case, after 7 iterations.

In the present case, it was desired to generate an m-sequence with 127 bits, which required a LFSR with length $m = 7$. The primitive polynomial for this purpose is, as table 2.1 shows, $x^7 + x + 1$, which means the feedback depends on the outputs of registers 1 and 7 and the resulting m-sequence will be register 7's output after $2^7 - 1 = 127$ iterations in the LFSR.

M-sequences serve multiple purposes, especially in the telecommunications field [23].

2.4.1 Properties of m-sequences

2.4.1.1 Balance Property

Let n_1 be the number of positions in an m-sequence with value "1"and n_0 the number of positions in the same m-sequence with value "0".

$$n_1 = n_0 + 1 \tag{2.2}$$

2.4.1.2 Run Property

A run is a subsequence obtained from the original sequence in which the bits are equal. It refers to a segment of the sequence where consecutive bits occur. The run property states that $\frac{1}{2^n}, \quad \forall\, n \geq 1$ runs will have length n, meaning:

- $\frac{1}{2}$ of the runs will have length 1;
- $\frac{1}{4}$ of the runs will have length 2.

These statements will not occur simultaneously. However, if at least one of them occurs, it can be considered an m-sequence. This property is very important for this study, as long runs are not desired as that would contribute to the learning phenomenon and thus, undermine the results obtained. The longer a run is, the less likely it is to be found in the m-sequence, which assures a minimized learning phenomenon.

2.4.1.3 Circular autocorrelation function Property

One curious feature of m-sequences is that their autocorrelation is a periodic delta function [25]. Autocorrelation, R_{xx}, is calculated as follows, where $x(k)$ is the sequence in question with delay in time $n = 0$:

$$R_{xx}(n) = \sum_{k=-\infty}^{\infty} x(k+n)x(k) \tag{2.3}$$

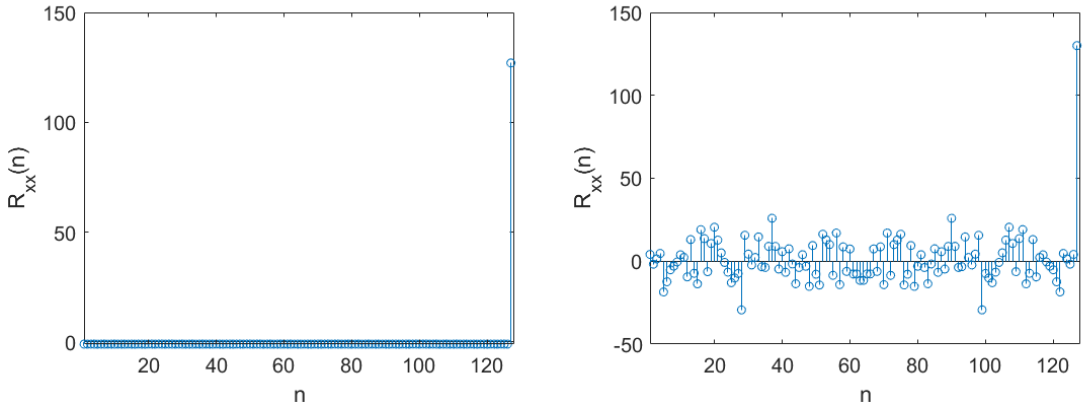

Function calculated for a 127-bit random sequence.

Figure 2.7: Auto correlation function of 127-bit sequences. (2.7a) Function calculated for a 127-bit m-sequence. (2.7b)

Figure 2.7 shows the autocorrelation calculated according to equation 2.3 for both an m-sequence (2.7a) and a random sequence (2.7b), both with 127 bits each, where n is the delay in time in equation 2.3. For an m-sequence, the maximum autocorrelation is 127 and it only happens for one value of n. For the rest of the values, $R_{xx} = -1$. In part, this is due to the Balance Property, which will result in almost the same number of -1 and 1 (when using NRZ) and thus, the total sum of the products will be -1. This property is very interesting to avoid learning on the part of the experimental subject, throughout the experiment . Not only that, but the mutual independence of shifted versions (different ns), enables the separation of the electrophysiological response of different stimulation sources and responses from different higher order kernels as well as allowing the study of the adaptive effects of previous occurrences [20].

2.5 Manchester encoding

Manchester encoding is widely used as a low-cost radio frequency transmission of digital data. It is a form of binary phase-shift keying and has allowed data encoding in a way that dismisses long strings of continuous zeros or ones, having the encoding clock rate built-in with the transmitted data. The difference to other methods of coding is that the bits "0"and "1"concern transitions and not static values, *i.e.*, one bit encodes a $1 \rightarrow 0$ transition and the other encodes a $0 \rightarrow 1$ transition [26]. This feature of Manchester coding is very valuable for this study in particular in order to avoid any habituation and polarization processes, especially whenever a sequence of equal bits in a row occur in the sequence shown, which would lead to several looking-like slides and thus, would originate more fixations than desired. As a result, it would be detrimental the study, because the saccadic movements would not occur as frequently.

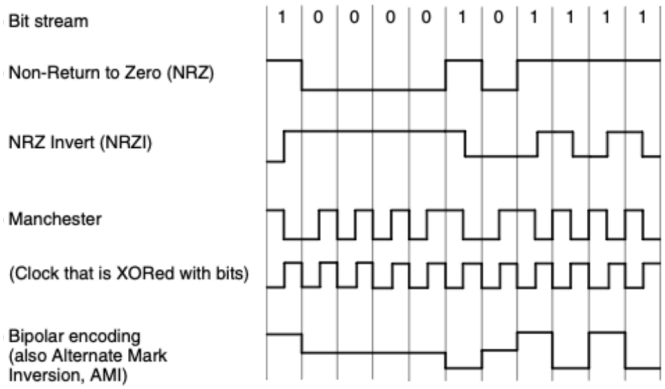

Figure 2.8: Comparison between different forms of encoding (adapted from [27]).

When using Manchester coding, the sequence increases twice in length, which leads to sequences with double the length when compared to the pre-coded sequence, as seen in figure 2.8 when comparing lines 1 (bit stream) and 4 (Manchester).

2.5.1 Non-return-to-zero (NRZ)

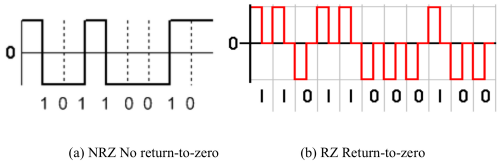

Figure 2.9: Non-return-to-zero and Return-to-zero representation in [28].

NRZ is a binary code in which ones are represented by one significant condition, usually a positive voltage, while zeros are represented by some other significant condition, usually a negative voltage, with no other neutral or rest condition, as opposed to return-to-zero (RZ), as seen in figure 2.9.

2.6 Inverting Schmitt trigger (IST)

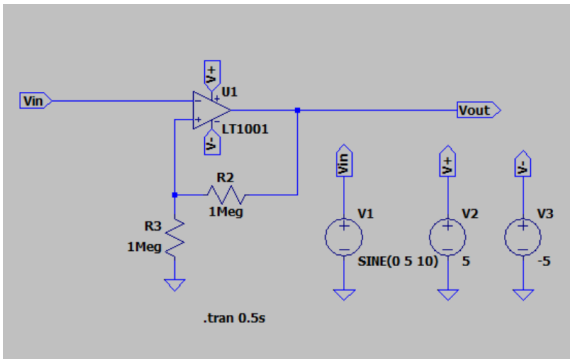

Figure 2.10: Equivalent circuit to the IST.

An IST is a type of Schmitt trigger that inverts the polarization as opposed to a regular Schmitt trigger. A Schmitt trigger is an example of a bistable multivibrator, which means it has two stable states. In order to change states, the circuit needs to be appropriately triggered. Bistable operation is due to a voltage divider in the positive feedback of an operational amplifier, as seen in figure 2.10.

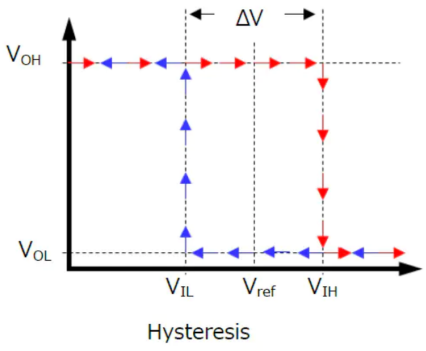

Figure 2.11: IST's transfer function.

Figure 2.11 shows the functioning of the IST. Schmitt triggers display hysteresis, as opposed to a comparator's transfer function. In the first case, there are two thresholds, V_{IL} and V_{IH}. It is only when V_{in} is above V_{IH} or V_{in} is below V_{IL} that a shift in the output occurs, resulting in less frequent changes when comparing to comparators. In the comparator case, there is only one threshold, i.e., V_{IL}=V_{IH}, so there is no hysteresis. This means every time the threshold is reached, there is a shift leading to much more frequent output variations and thus, making it much less stable.

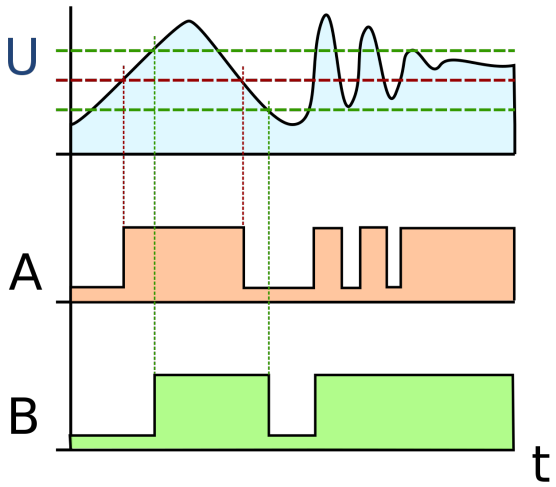

Figure 2.12: Comparison between a comparator and a Schmitt trigger circuit. **U** - input; **A** - comparator's output; **B** - Schmitt trigger's output.

Figure 2.12 shows the difference in the output between a comparator (A) and a Schmitt trigger (B). The horizontal green and red lines show the thresholds for each circuit (the green lines represent the Schmitt trigger's thresholds and the red line represents the comparator's threshold). It is clear that the comparator circuit shows much more sensitivity to shifts in the output as opposed to a Schmitt trigger circuit. Not only is the comparator circuit more prone to shifts but is also more sensitive to noise, which is undesirable considering there might be changes in the current throughout the experiment, which cannot be controlled due to the fact that only the test subject is inside the Faraday cage (FC), and so, the output must be as stable as possible.

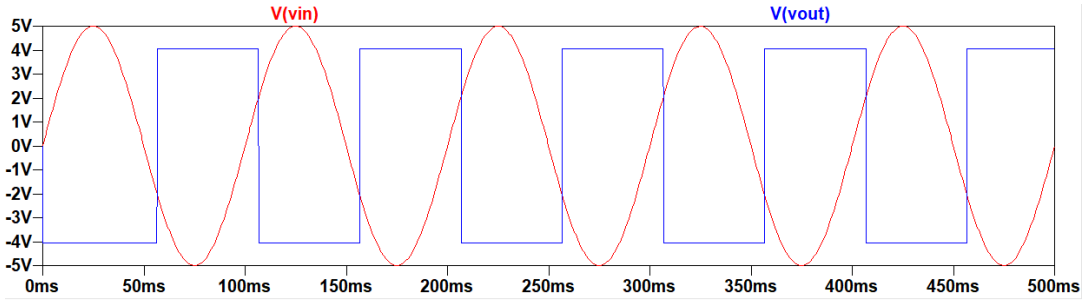

Figure 2.13: IST's waveform. Red line - input; Blue line - output.

In the IST's case, the opposite happens. The thresholds still control how the output shifts but in the opposite polarization, so that if the Schmitt trigger's output was to be high, the IST's output would be low and vice-versa.

2.7 Binary Symmetric Channel

A general communication system has been already introduced in section 1. Figure 2.14 shows a similar communication system as figure 1.1, where the transmission is polluted by noise, which

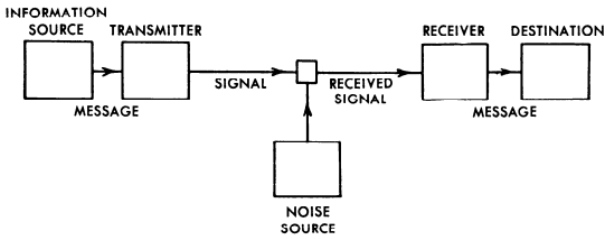

Figure 2.14: General communication system (adapted from [29]).

tends to occur in most cases. Therefore, when the message reaches the receiver, the signal has embedded noise. The channel is seen as the form used to transmit the message encoded from the transmitter to the receiver. The receiver does the opposite of a transmitter, decoding the message [29].

In the simplest case, the channel can be binary, as in the values transmitted are "0"or "1", *i.e.*, binary symbols [30]. The transmission could be either symmetric or asymmetric, depending on the relation between p and q, which are the probabilities of the transmitted symbol being "1"and received symbol being "0"and the transmitted symbol being "1"and the received symbol being "1", respectively.

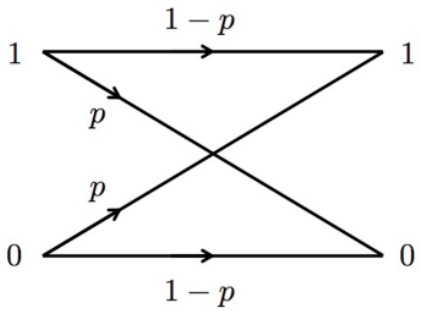

Figure 2.15: A binary symmetric channel.

In figure 2.15, the symmetric case is represented. A binary channel is symmetric whenever $p, q \in [0; 1] : p = q$. Otherwise, *i.e.*, if $p \neq q$, the binary channel is asymmetric [31].

In this work, the channels were considered to be symmetric, thus the only probability concerned is p, making p(1|0)=p(0|1)=p.

$$p(y|x) = \begin{cases} 1-p & \text{if } y = x \\ p & \text{if } y \neq x \end{cases} \tag{2.4}$$

In equation 2.4, the probabilities of transmission of the binary symmetric channel are summarized. To each channel, there is a value of capacity, which is the ability of transmission of information in the said channel from the source, in bits per transmitted symbols.

$$C_{BSC} = 1 - H_b \tag{2.5}$$

Equation 2.5[32] shows how to obtain the capacity for a channel, which depends directly on the binary entropy of said channel, H_b.

$$H_b(p) = p \log_2 \frac{1}{p} + (1-p) \log_2 \frac{1}{1-p} \tag{2.6}$$

Equation 2.6 [31] shows how to obtain the binary entropy for a given crossover probability p, which can also be called the uncertainty [32].

2.8 Matched filters

A matched filter is a tool used in signal processing in order to extract a known wavelet $s(k)$ (a template) from a signal embedded in noise $n(k)$ [33]. It is implemented by convoluting the signal with noise $(s(k) + n(k))$ with the time-inverted version of the wavelet $s(t)$. One of the advantages of using such filtering is that it maximizes the SNR in the presence of additive white gaussian noise (AWGN) [34], which will happen when the filter's impulse response is the time-inverted wavelet [33]. This technique, however, is not as useful if the waveforms are unknown [35].

$$y[n] = \sum_{k=-\infty}^{\infty} h[n-k]x[k] \tag{2.7}$$

Equation 2.7 shows the output of the matched filter $y[n]$ when applying the linear filter $h[x]$ to the input signal $x[k]$. Matched filtering in conjunction with Neural Networks (to assess the matched filter's performance) has already been used to detect spikes in pediatric (but also with potential use in adult) EEG with the aim of aiding in detecting epileptic spikes, with a sensitivity of 99.96% [35]. This shows the possible application of matched filtering, especially if used in a more-than-one-phase detection model, in detecting other neurological pathologies.

2.9 Hamming distance

Hamming distance concerns the number of differences between two sequences of symbols [36]. In other words, it is the number of symbols that need to be flipped in a word a in order to be identical to a word b.

This concept is used in error detecting and correcting codes. Error-detecting and error-correcting come in sequence of information transmission, throughout the process of decoding information. In order to perform good correction codes, the error rate must be $\leq 25\%$. If it is $= 50\%$, inverting the bits will still result in an error $= 50\%$, which will make it impossible to correct the word obtained.

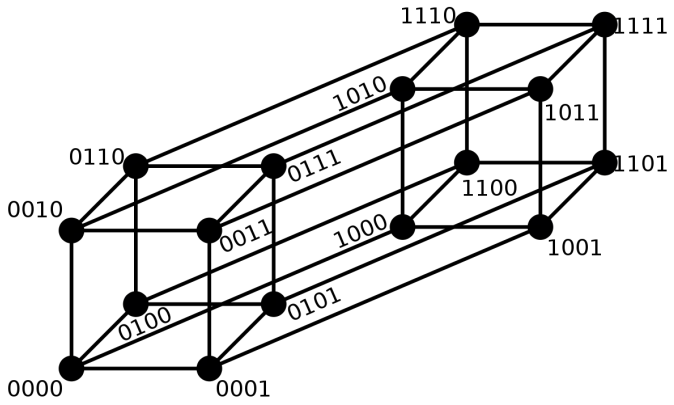

Figure 2.16: Hamming distance three-dimensional representation of 4-bit binary sequences.

Figure 2.16 shows the three-dimensional representation of 4-bit binary sequences, where each edge represents one unit in the Hamming distance. For instance, the Hamming distance between sequences "0000"and "0110"is 2, as they are separated by two edges.

CHAPTER 3

LITERATURE REVIEW

3.1 The use of m-sequences and matched filters in neuroscience

Table 3.1: Summary of the literature review of the techniques used in this work.

Authors	Year	Dataset	Aim	Results/conclusions	Future work
Hatzilabrou, G. M. Greenberg, N. Sclabassi, R. J. Carroll, T. Guthrie, R. D. Scher, Mark S. [37]	1994	two preterm and fullterm neonates	To compare the effectiveness of a technique for detecting REM in newborns that uses four criteria thresholds with a technique that uses only 2 and then with the application of other one that uses a REM signal as a template.	The matched filter proved to be more effective in detecting REM than the other techniques techniques when applied to newborns.	-

Bell, S. L. Allen, R. Lutman, M. E. [38]	2001	20 (10 male + 10 female) subjects, mean age= 24.3 years, otologically normal	To prove the efficacy of using M-sequences in the study of MLR (middle latency response) in order to decrease the acquisition time in the evaluation of the depth of anesthesia, since the conventional technique has a longer duration than desirable given the rapid changes in this parameter.	MLS (maximum length sequences) can be used with confidence in MLR acquisitions. The best MLS to use are those of order 4 due to better SNR.	To study the effect of MLS on wave latencies in addition to MLR in the different phases of anesthesia for its use in the assessment of anesthesia depth.
Völk, Florian Straubinger, Martin Roalter, Luis Fastl, Hugo [39]	2009	28 year old male subject	To demonstrate an algorithm for measuring HRIRs (head related impulse responses) that uses MLS and ESS (exponential sine weep).	It is possible to apply MLS in conjunction with ESS to measure HRIRs in studies in psychoacoustics.	-
Stamoulis, Catherine Chang, Bernard S. [40]	2009	3 patients with multifocal seizures	To assess the possibility of using matched filters to locate sources of epileptic seizures from acquisitions.	It was possible to use matched filters to separate components from different foci during an epileptic seizure based on their patient characteristics and arrival times between electrodes.	Validation of the method is required but it shows promise.

Y Nishitani, C Hosokawa, Y Mizuno-Matsumoto, T Miyoshi, H Sawai, S Tamura [24]	2012	6 cultured cell samples with dissociated hippocampal neurons at 22-50 days in vitro	To confirm the assumption that some LFSR are found in neuronal networks in control of the communication of information that use m-sequences.	More 7-bit sequences were detected in time series where spikes were used than in random time series, suggesting that there are LFSR-equivalent circuits of length 3 in neuronal networks which generate the detected m-sequences.	To identify the location and type of LFSR in order to understand why 3-stage LFSR are specifically detected. To analyze the correlation between the culture term and the number of detected sequences and also the correlation between this number and the scale of neural networks.
Janacsek, Karolina Shattuck, Kyle F. Tagarelli, Kaitlyn M. Lum, Jarrad A.G. Turkeltaub, Peter E. Ullman, Michael T. [41]	2020	20 studies used in meta-analyses (participants) and 627 participants for ALE (activation likelihood estimation) analyses.	To understand which structures are involved anatomically in sequence learning in humans.	The basal ganglia (globus pallidus) and anterior parts of the putamen and caudate nuclei (striatum) are involved in the early stages of learning, i.e., regarding sequential order learning. The ventral premotor cortex is in charge of sensorimotor functions. The VI lobe of the cerebellum is in charge of the attention/working memory functions.	To expand the focus on the basal ganglia beyond the striatum, to include the globus pallidus.

Müller, Philipp L. Meigen, Thomas [20]	2016	no data set as it was a review article	To show the potential of m-sequences in multifocal ophthalmic electrophysiology (multifocal ERF and VEP).	M-sequences make it possible to separate the captured responses according to different locations in the visual field, as well as allowing to analyze adaptation effects of previous events. Multifocal techniques such as mfERG make it possible to distinguish hereditary diseases. Changes in patients in mfERG with diabetes occur before structural changes in diabetic rhinopathy, and in the case of glaucoma, reduced amplitudes with defects in the field of vision and nerve fiber thickness before the onset of the disease are observed, which shows mfERG has benefits for early diagnosis of the disease.	-

3.2 Conclusion on literature review

As seen in the previous section, both m-sequences and matched filters have not been deeply studied in the neurological field. Matched filters proved to be an effective tool for detecting REM in EEG signals as well as locating sources of epileptic seizures. M-sequences have also proven to serve various applications to study the effects of anesthesia, in psychoacoustics and in electrophyisiology, which opens the door for its use in the study of other neurological diseases.

With this in mind, in this dissertation, a model of the brain was proposed using saccades, measured by EEG and EOG. These saccades were stimulated using a slide show built from an m-sequence and using only the EEG and EOG signals, was there an attempt to retrieve

the original sequence. To do so, matched filters were used to detect the bits and estimate the sequences for each channel. At last, the patterns in recognition were assessed, which in the future could serve to infer as to the presence or absence of pathology when investigating between healthy and unhealthy subjects.

Chapter 4

Materials and Methods

This chapter is divided in four sections, as outlined below:

Section 4.1 - Subjects - A brief description of the experimental subjects.

Section 4.2 - Experimental design - A description of the experimental design, namely regarding the conversion of the m-sequence into the slideshow presented throughout the acquisition;

Section 4.3 - Acquisition - It describes the acquisition process, namely, the sampling rate, the number of electrodes and their positioning on the experimental subject, in addition to what the experiment consisted of;

Section 4.4 - Processing - It describes how the acquired data were processed in order to perform the detection and estimation of the sequences for every channel. As mentioned before, a Data Science Pipeline-approach was used, meaning it consisted in a sequence of scripts, each performing a specific task. This process is explained in detail in this section and summarized in the appendix section B.

4.1 Subjects

Table 4.1: Data for the 6 experimental subjects.

Acquisition	Age	Sex	Dominant hand	Glass wearer	No. of coffees / day	Medication
M11FA	24	Male	Right	No	4	No
M11FB	24	Male	Right	Yes	1	No
M11FC	25	Male	Right	Yes	2	No
M11FD	21	Male	Right	Yes	3	No
M11FE	22	Male	Right	No	1	No
M11FF	24	Male	Right	No	1	No

The experiment was run in 6 subjects, in total. Their main information is summarized in table 4.1. The subjects were on average 23 years old, healthy, with no psychological pathology or other kinds.

4.2 Experimental design

The acquisitions took place inside an electromagnetic field shielded room in the Propagation and Radiation Lab of the Department of Electrical and Computer Engineering (DEE) in the facilities of NOVA School of Science and Technology (FCT NOVA). Throughout the experiment, the subjects were alone inside the room, with the switchboard and lights off. They were instructed to look at the slides presented on the screen, namely and solely at the circles that would either be on the left or right of it. They were instructed to not make any other sort of facial and body movement besides saccades so as not to corrupt the EOG with motion artifacts. In the first slides, there were more than one circle in order to centralize the gaze of the subject, similarly to a regular VGS study. It took approximately 3 minutes.

4.2.1 Slides

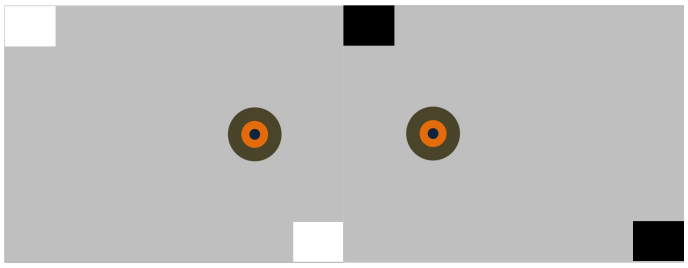

a b

Figure 4.1: Bit "0"in the m-sequence after Manchester and NRZ codification.

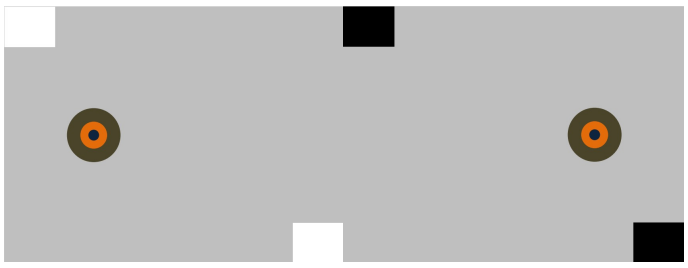

a b

Figure 4.2: Bit "1"in the m-sequence after Manchester and NRZ codification.

The slides used to build the final sequence shown to the subjects are presented in figures 4.1 and 4.2. The workflow shown in figure 1.2 shows that in order to transmit the m-sequence,

there is a need to encode it, using Manchester, in this case. In Manchester encoding, each bit in the original sequence translates in a transition between two slides. It was defined that each bit in the original sequence leads to a transition from a slide with white squares on the corners to a slide with black squares on the corners, as seen in figures 4.1 and 4.2.

Bit "0"in the original sequence will result in a transition from a slide with a circle on the right to a slide with a circle on the left and bit "1", vice-versa. In the event that there are multiple identical bits or runs of bits in a row in the original sequence, although avoided by the use of m-sequences, the use of Manchester coding will prevent fixation movements, which go against the scope of the study, since the goal was to study saccadic movements.

The slides were presented in a laptop with no network connection at a distance of 100 cm from the subject. As for long distance saccades ($\approx$ 150 cm) in adults, the latency is $\approx$ 250 ms [42], the duration of the slides was set to 850 ms, which was enough time to obtain a reliable response to the stimuli. Because the original m-sequence had 127 bits of length, after Manchester encoding, the final sequence had 127 pairs of slides, i.e., 254 slides. Four slides were added in the beginning to ensure the sequence would only be presented to the subject once they were alone. One final slide was presented to ensure each slide of the sequence had the same recorded response time. In total, the slide show presented had 259 slides. The same slide show was presented to every subject, i.e., the m-sequence was the same throughout all the experiments. Using m-sequences contributes to reducing the learning phenomenon, which would also be detrimental to the study because it could affect the signals measured.

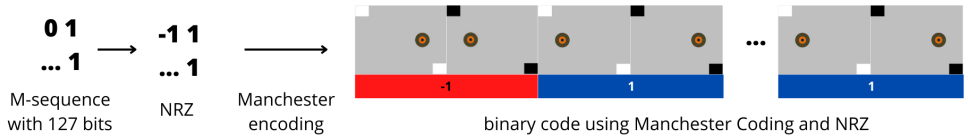

Figure 4.3: Summary of the m-sequence's conversion to slides.

4.3 Acquisition

In each acquisition, there were 8 electrodes for each kind of signal, i.e., EEG and EOG, which means, for every subject, there were in total 16 electrodes distributed over the scalp, face and wrists. Because the aim was to explore the signals in order to extract as much information as possible, the intention was to ensure no part of the signal was left out so the sampling rate (f_s) used was 16384 Hz, as it is the maximum frequency allowed by BioSemi's ActiveTwo, the data acquisition system used.

4.3.1 EEG

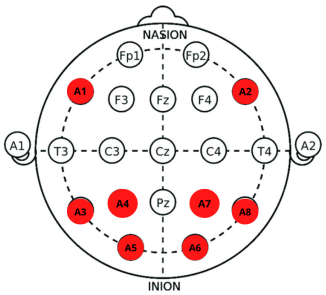

Figure 4.4: Electrodes' positioning for EEG collection.

To collect the EEG data, 8 pin electrodes were used in a standard 256-hole EEG cap. The electrodes were positioned as seen in figure 4.4, with two electrodes in the frontal lobe, four electrodes in the parietal lobe and two electrodes in the occipital lobe, where the visual cortex is situated. The lobes other than the visual cortex were also investigated in order to look for relevant information, since this was an exploratory work.

4.3.2 EOG

For the EOG acquisitions, 8 flat type electrodes were used, positioned as follows:

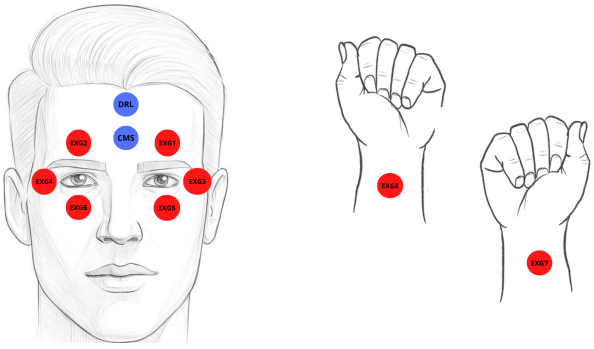

a Positioning on the head. b Positioning on the wrists.

Figure 4.5: Electrodes' positioning for EOG collection.

As seen in figure 4.5a, six electrodes were positioned around the eye area in order to study both the horizontal and vertical saccadic movements. Two other electrodes were positioned in the forehead: driven right leg (DRL) (on the top) and common mode sense (CMS) (on the bottom). These electrodes are used by the equipment as a reference and replace the ground electrode used in conventional systems. As seen in figure 4.5b, two other electrodes were positioned, one on each wrist, whose signal was mostly dominated by electrocardiogram (ECG).

ECG, although no the focus of the dissertation, was thought to be an interesting signal as some malfunctions in the heart can be linked to higher risk of developing some neurological

diseases. For instance, coronary heart disease and heart failure might be linked to a higher risk of dementia [43] and impaired heart rate variability may also be considered a marker for differentiating dementia with Lewy bodies (DLB) from Alzheimer's disease (AD) [44].

4.4 Processing

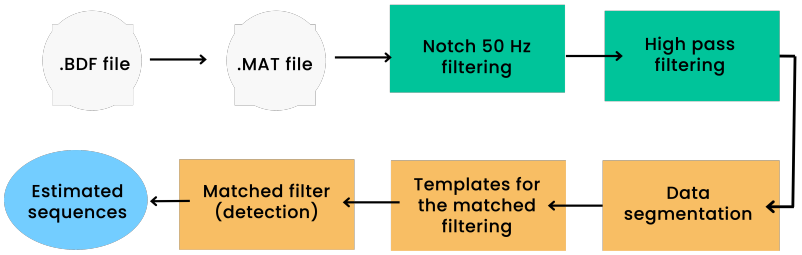

Figure 4.6: Workflow for the processing of the data.

Figure 4.6 shows the workflow used in the processing stage. The information collected in the acquisition was stored in a .bdf file, containing the 16 channels in which the signals were measured, plus the Status channel, where the information coming from the visual stimuli is stored. The processing stage can be seen as two major tasks:

1. the filtering of the data in order to remove the noise coming from the grid which is located at 50 Hz using a bandstop filter, as well as the high pass band, because the goal was to analyze patterns in the signal above certain frequencies;

2. the matched filtering in order to detect the bits and estimate the sequence for each channel and compare it to the original sequence in order to assess detection of the correct sequence.

In order to develop the software, 4 acquisitions were made, with different numbers of electrodes, electrode positioning and/or number of bits in the m-sequence presented:

- M11A - 8 electrodes for EEG + 8 electrodes for EOG (127 bits)
- M11B - 0 (zero) electrodes for EEG + 2 electrodes for EOG (127 bits)
- M11D - 0 (zero) electrodes for EEG + 8 electrodes for EOG (255 bits)
- M11E - 0 (zero) electrodes for EEG + 8 electrodes for EOG (127 bits)

4.4.1 Storing the stimuli's information in the .bdf file

The information from the visual stimuli was stored in the last channel of the .bdf file, the Status channel. In this channel, the information is stored in a binary format, with 24 bits, each one concerning each of the 16 trigger inputs as well as other inputs in the ActiveTwo USB receiver, situated outside the room where the acquisitions took place. These are connected through an optic fiber cable. The information from visual stimuli over time is stored in Trigger inputs 2 and 3 in the USB receiver. Connected to these trigger inputs, are two phototransistors, each regarding each trigger input, that detect the light coming from the screen as the slideshow goes by. These phototransistors are placed on top of the squares shown in figures 4.1 and 4.2, on the screen during the acquisition.

As seen in these figures, each bit is located in a transition from a slide with white squares to a slide with black squares. In the Status channel, this will be detected as a down transition by the transistors. Therefore, it can be said that the bits in the original sequence are located in the down transitions of the transistors.

Again, as seen in figures 4.1 and 4.2, there are two squares in each slide, each square regarding each transistor. This way, the data in each channel can be segmented bearing the transitions of the phototransistors in mind.

However, direct connection was not possible because it was desired that whenever a phototransistor detected light, its trigger input would have value "1"and in the opposite case, value "0". Due to light detection, what happens is that the transistor is in active mode, which leads to electric current flow and causes the measured potential in the trigger input to be low, contrary to what is intended. With that in mind, a circuit was built using an IST, in order to invert the polarization and so, obtain the desired result. In that circuit an LED was also connected to each transistor so that it would indicate detection of light so, before each acquisition, this photo-detection could be assessed right away without needing to check the acquisition software.

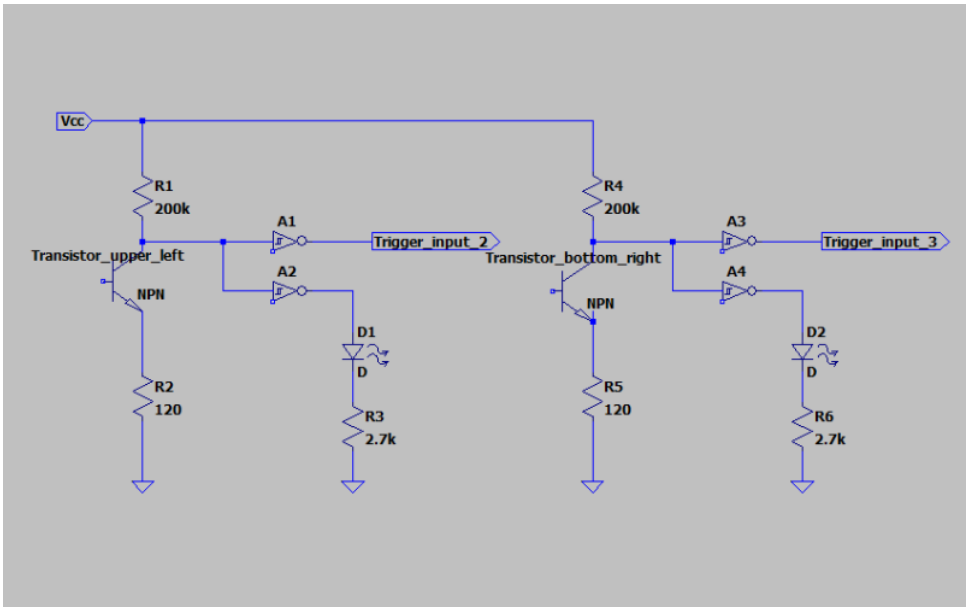

Figure 4.7: Circuit used to process the photo transistor's information.

Figure 4.7 shows the final circuit. It can be divided into two subcircuits, each relative to each phototransistor. Each subcircuit gets the input from the detection in the phototransistor. Its output is connected to two ISTs, whose outputs will be the Trigger inputs, to be stored in the Status channel, and an LED that is ON whenever light detection occurs and OFF whenever it does not. In the circuit above, each phototransistor is represented by a regular NPN transistor with the base left open circuit, as LT Spice, the software used to perform the simulation, did not have any models as far as phototransistors are concerned.

The .bdf file was converted to a .mat file using EEGLAB toolbox (Delorme and Makeig, 2004). The algorithm for the processing was developed in MATLAB. Firstly, the data in the .mat file, obtained from EEGLAB, was split into 16 variables, regarding the 16 channels recorded to ease the processing using *Faz03Data*χ*.m*, which resulted in file *Data*χ*bEx1to16*.

4.4.2 Filtering

All the filters used throughout the processing were of digital kind. To design the filters, the function `fir2` was used in MATLAB, which creates finite impulse response filters recurring to the frequency sampling method.

4.4.2.1 Bandstop filter 50 Hz

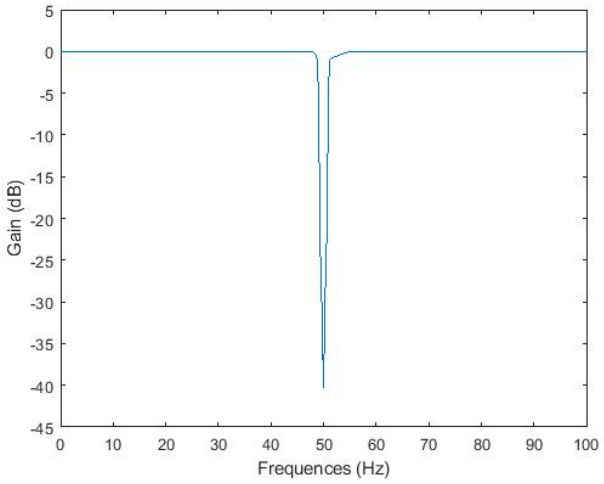

Figure 4.8: Band-stop filter used to filter out the 50 Hz noise.

A digital filter of order 81920 was used, which allowed for more precise removal of the 50 Hz frequency (corresponding to the grid frequency), that often causes noise, while also keeping the closest frequencies to this one with less significant attenuation, as seen in figure 4.8. The order of the filter was obtained doing $\frac{f_s}{2} \times 10 = \frac{16384}{2} \times 10 = 81320$. The sampling rate was divided by 2 because of the Nyquist theorem, that states that the f_s should be at least twice the maximum frequency of the signal, which means the maximum frequency should be $\frac{f_s}{2}$ at the most. For each "frequency", it was selected a factor of 10 for the points used to achieve better precision in the filter.

The notch 50 Hz filtering was performed by function `Faz04Filtra50HzDataNew` resulting in file *DataχEx1to16*.

4.4.2.2 High pass band filtering

As for the high pass band filters, 4 cutoff frequencies were chosen according to the dominance in the FFT of one of the acquisitions used in the development of the algorithm, namely, M11E:

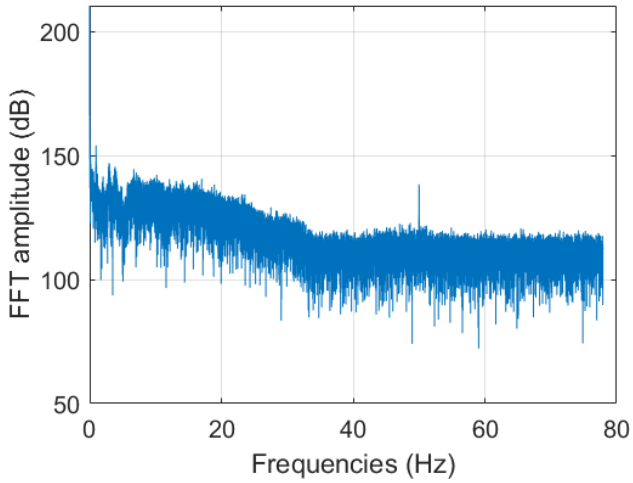

Figure 4.9: FFT of EXG8 electrode on acquisition M11E.

Figure 4.9 shows the result of FFT on one of the acquisitions used to develop the algorithm. The frequencies with the highest amplitudes are situated on the lowest range (0-30 Hz). There is also a peak on 50 Hz, belonging to the frequency associated with the power grid.

Having this in mind, the maximum cutoff frequency chosen to be analyzed was 30 Hz, because if higher, most of the signal would be mitigated and no interesting information would be left. The 30 Hz high pass band was chosen to study the typical responses in case the detected signal had no human source, in order to compare it with the other high-pass bands.

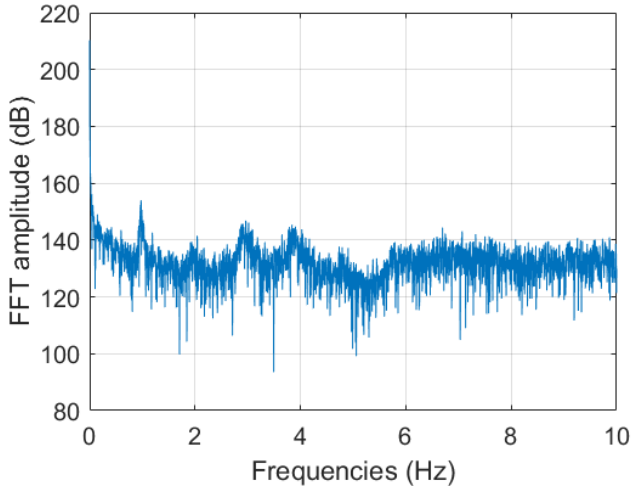

Figure 4.10: FFT of EXG8 electrode on acquisition M11E (0-10 Hz).

As seen in figure 4.10, one of the frequencies with the highest amplitude is 1 Hz, so in order to keep it, a cutoff frequency of 0.5 Hz was chosen. Frequencies 3 and 4 Hz are also of high amplitude, so a filter with cutoff frequency 2 Hz was chosen.

Taking all this in consideration, the cutoff frequencies chosen were the following:

- 0.5 Hz (the detailed design of this filter can be accessed at I.1);

- 2 Hz (the detailed design of this filter can be accessed at I.2);
- 10 Hz (the detailed design of this filter can be accessed at I.3);
- 30 Hz (the detailed design of this filter can be accessed at I.4).

Each high pass band filtering was performed by a function called `Faz05FiltraHP`f`DataNew`, where f is the value of the cutoff frequency in question, resulting in *Data*χ*fEx1to16*. The parameters for each filter for function `fir2` can be seen in section I.

4.4.3 Matched filtering - detection

4.4.3.1 Data segmentation

The data was divided into segments of 350 ms (5734=f_s*0.350 samples each) starting with an instant of a down transitions of the transistors, i.e., where the bits of the original sequence were located. In order to obtain the designated segments:

1. `FazA01InfoTransistors.m` used the information in the .bdf file to obtain two .mat files which contained the information concerning the state of each transistor throughout the experiment, in binary, directly from the Status channel: *kuo8Green* and *kuo8Red*;
2. `FazA02Conta259Slides.m` worked as the software's checkpoint to confirm the validity of the acquisition: using *kuo8Green* and *kuo8Red*, it checked if the number of slides registered in both files matched the expected number of slides, i.e., 259 and, if positive, it renamed them to: *kuo8Green259* and *kuo8Red259*, respectively. If not, it renamed them to *kuo8Greenxxx* and *kuo8Redxxx*, respectively, and the algoritm would be terminated;
3. `Faz06SpotLocs.m` used *kuo8Green259*, i.e., the information regarding the transistor in the upper left corner of the screen, to obtain the locations of the transitions of said transistor, resulting in a .mat file with 3 variables (*ki32UpLocs* (containing the location of up transitions), *ki32DwLocs* (containing the location of down transitions) and *ki32AllLocs* (containing the locations of all transitions)): *SpotLocsUpDwAll*χ;
4. `Faz07Segments.m` used the information in the variable *ki32DwLocs* from *SpotLocsUpDwAll*χ to divide each channel in the filtered data (*Data*χ*fEx1to16*) into segments with 350 ms of duration that start whenever a down transition occurs, i.e., when a new bit from the sequence starts. This resulted in file *rSegmentsG1To16*, which contained in total 16 variables, regarding each of the 16 channels recorded. Each channel is represented by a matrix with 127 rows corresponding to the 127 bits of the sequence to be estimated, each having 5734 columns (length of each segment, corresponding to 350 ms).
5. `FazA08CalculaDiferenciais.m` obtained the differential channels by calculating the subtraction between the 16 channels, which resulted in 136 channels in total. In doing so, it can be assessed if there is useful information in the differential channels and in addition to the unipolar channels. Of this function, resulted file *AllSegments.mat*.

4.4.3.2 Templates for the matched filtering

1. `FazA09Normaliza.m` normalized the channels in *AllSegments.mat*, making sure all the segments had an average equal to zero and energy equal to 1. This resulted in file *rMESegments.mat*.

2. `FazA10Sondas.m` calculated the templates to be used in the matched filtering by temporal summation. It generated two templates for each channel, a template to estimate bit "1"and a template to estimate bit "0". In order to obtain these templates, all the segments that corresponded to a position in the original sequence to "1", were summed to obtain the template for "1"and the rest of the segments were used to obtain the template for "0", for each channel. In total, there were two templates for each of the 136 (16+120) channels. These were normalized after summation and resulted in file *Sondas.mat*. This function used an auxiliary function, `fazSondas`, which produced the two templates for each channel: $|SondaA_n^1\rangle$ and $|SondaA_n^0\rangle$, where n is the number of the channel, $n \in \{0, ..., 136\}$.

4.4.3.3 Matched filtering (detection)

To perform the matched filtering, function `FazA11Detecao` calculated the inner product between every segment of each channel and each of the templates, using an auxiliary function, `acertosSequences`.

This function took 4 arguments: the matrix with the normalized segments for each channel, $\langle rmeSegmentsA_n|$, in *rMESegments.mat*, both templates (normalized), $|SondaA_n^1\rangle$ and $|SondaA_n^0\rangle$ and $OriginalSequence$,a 127x127 matrix, with the original set of m-sequences, where each line corresponded to a 127-bit m-sequence. Each original m-sequence in the original set was represented by $\langle OriginalSequence_l|$, where $l \in \{1, ..., 127\}$, standing for the 127 m-sequences in the original set.

In order to perform the detection, the inner product was calculated for each segment $\langle rmeSegmentsA_n^m|$, $m \in \{0, ..., 127\}$ in each channel $n \in \{0, ..., 136\}$, with both templates, $|SondaA_n^1\rangle$ and $|SondaA_n^0\rangle$:

$$\langle rmeSegmentsA_n^m|SondaA_n^1\rangle = Estimador_n^m UM$$

$$\langle rmeSegmentsA_n^m|SondaA_n^0\rangle = Estimador_n^m ZERO$$

For all $m \in \{0, ..., 127\}$ segments in $n \in \{0, ..., 136\}$, two estimators are obtained, concerning the correlation for each bit for said segment m.

In order to estimate the sequence for each channel n, for every position m, the correlation for each value of bits, "1"and "0", were compared and whichever were the highest, would be considered the value for said position. In the end, each channel had an estimated sequence with 127 bits, in a column vector.

In order to obtain the number of hits, once again, the inner product was used. The inner product was calculated between each m-sequence $l \in \{1, ..., 127\}$ in the original set, $\langle OriginalSequence_l|$, and the estimated sequence of each channel $n \in \{0, ..., 136\}$, $|Estimated\ sequence_n]\rangle$.

At this stage, because the m-sequence was coded in NRZ, every time a hit between the original set and the estimated sequence occurred, it would add up to 1 so in the end, a balance for each pair original sequence - estimated sequence was obtained. In the end, `acertosSequences` revealed the number of hits for every channel for each sequence $l \in \{1, ..., 127\}$ in the original set. These were represented in a table for every pair acquisition-high pass filter.

Chapter 5

Results and Discussion

There were 136 channels for each pair acquisition-high pass band. In the end, the algorithm obtained a row vector for each channel with the number of hits when comparing the estimated sequence in it with each of the sequences in the original set. These rows were placed in a table to ease the analysis, similar to table in annex II.

The total number of hits for each m-sequence was, of course, 127, as this was the number of bits in the sequence. The detection for each sequence was considered to be positive if the number of hits was superior to 95 ($75\% \times 127 \approx 95$) for a sequence in the original set. The detection was at a subject level, i.e., it took in consideration the number of channels where the retrieval had been considered successful, and not at a sequence level, i.e., the number of hits for each estimated sequence, obtained for each pair "original m-sequence-channel". So, the maximum number of successful retrievals (detections) was 136, because, for each case, there were 136 channels to be analyzed for each pair acquisition-high pass band, i.e., there were 136 chances to estimate the m-sequence.

5.0.1 High pass band - 0.5 Hz

Table 5.1: Successful retrievals in the 0.5 Hz high pass band.

	M11FA	M11FB	M11FC	M11FD	M11FE	M11FF
No. of channels with hits=127	76	114	99	107	45	99
Percentage of channels with hits=127	56%	84%	73%	79%	33%	73%

In the 0.5 Hz high pass band, all EEG's characteristic waves are present. In this analysis, only m-sequence 11 registered a number of hits superior to 95, i.e., only this sequence was detected. This coincides with the m-sequence used to prepare the slideshow.

5.0.2 High pass band - 2 Hz

Table 5.2: Successful retrievals in the 2 Hz high pass band.

	M11FA	M11FB	M11FC	M11FD	M11FE	M11FF
No. of channels with hits=127	52	116	100	107	32	97
Percentage of channels with hits=127	38%	85%	74%	79%	24%	71%

In the 2 Hz high pass band, all EEG's characteristic waves are present. In this analysis, only sequence 11 registered more than 95 hits. Again, it coincides with the sequence shown to be displayed.

5.0.3 High pass band - 10 Hz

Table 5.3: Successful retrievals in the 10 Hz high pass band.

	M11FA	M11FB	M11FC	M11FD	M11FE	M11FF
No. of channels with hits=127	102	120	110	118	103	113
Percentage of channels with hits=127	75%	88%	81%	87%	76%	83%

In the 10 Hz high pass band, only α and β rhythms are present. In this analysis, only sequence 11 registered more than 95 hits.

5.0.4 High pass band - 30 Hz

Table 5.4: Successful retrievals in the 30 Hz high pass band.

	M11FA	M11FB	M11FC	M11FD	M11FE	M11FF
No. of channels with hits=127	136	133	123	130	136	136
Percentage of channels with hits=127	100%	98%	90%	96%	100%	100%

In the 30 Hz high pass band, only β rhythms were present. In this analysis, only sequence 11 registered more than 95 hits.

5.1 Discussion

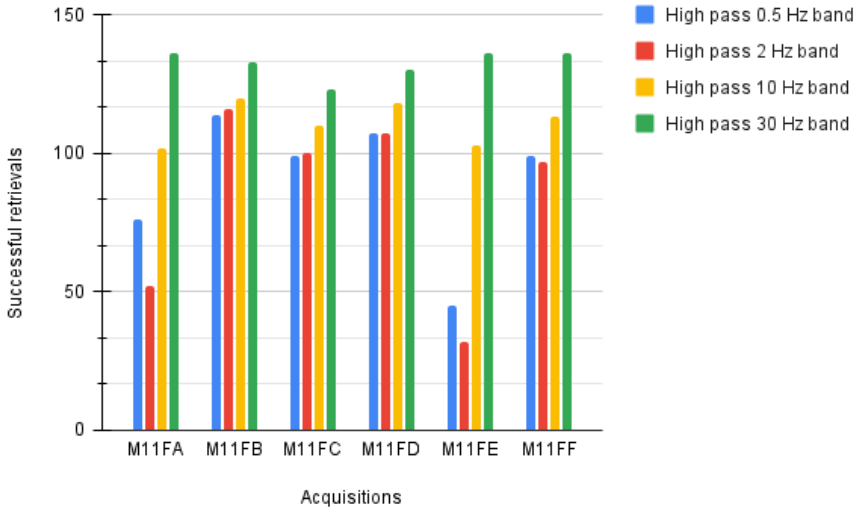

Figure 5.1: Summary of the results presented above.

Figure 5.1 shows the number of channels for each pair "acquisition-high pass band"in the test set. This represents the number of detections, which only happened for m-sequence 11, in every channel tested. In all acquisitions, the m-sequence was detected, although acquisition M11FE showed lower detection rates for 0.5 and 2 Hz-cutoff frequencies (33% and 23%, respectively).

A general increase in the number of detections can be noticed as the cutoff frequency increases. Furthermore, the algorithm was tested for signals filtered with a high pass band filter with a cutoff frequency of 150 Hz and it was observed that the number of detections kept increasing (it proved to be a high enough cutoff frequency to register a 100% rate of detections), which overall proves this tendency for the number of detections to increase as the cutoff frequency increases as well.

This is in line with what is observed in figure 4.9, because above 30 Hz, the signal is negligible, so in this band, there seems to be no human component signal, which gives rise to maximum detection rates. It seems that the more physiological component there is in the signal, the more "disturbances"to the system seem to be taken into consideration, which may point to a deviation from what happens when testing higher cutoff frequencies.

It can be concluded that the higher the cutoff frequency used in the high pass filter when analyzing experimental subjects, the closer it gets to a signal with no human component at all, which shows the algorithm's ability to detect the m-sequence effectively.

For three of the acquisitions (M11FB, M11FC, and M11FD), the successful retrieval rates were approximately the same for the first two cutoff frequencies, which may show redundancy in these cases and no significant components are situated in frequencies below 2 Hz in those cases.

A general increase in successful retrieval rates can be seen when rising the cut-off frequency from 2 Hz to 10 Hz, which shows that, generally, the latter seems to be a low enough frequency for the m-sequence to be detected with a substantially high successful retrieval rate.

It is worth noting, however, that in half of the subjects (M11FB, M11FD, and M11FF), the software predicted the sequences with a 100% hit rate for some channels, which was not in line with what happened in the other half of the acquisitions: for M11FB, it happened 27 times when using the first cutoff frequency and one time when using the second one. For M11FD, it happened 5 times for the third cutoff frequency and 14 times for the last one. Finally, for M11FF, it happened twice for the second cutoff frequency, 14 times for the third, and 15 times for the last one. When analyzing in which channels this had happened, no conclusions could be drawn as to whether this had been due to a malfunction in the electrodes because it differed from acquisition to acquisition and from high pass band to high pass band. However, it should be noted that before every acquisition, the impedance relating to each electrode was checked and confirmed to be low and no abnormalities in the positioning of the electrodes were recorded.

For the acquisitions M11FA, M11FE and M11FF, the tendency for the number of hits to increase with increasing cutoff frequency only applied to a certain extent. In this case, there was a decrease in the number of hits, followed by an increase. In two of these acquisitions, when filtering the data with a 30 Hz-cut-off high pass filter, the hits were equal to the total number of channels, which may indicate that no signal from the subject remained in the data analysis at that point, resulting in a successful retrieval rate of 100%.

In general, it can be observed that the higher the cutoff frequency used in the high pass analysis, the closer to a 100% rate of successful retrieval is reached, which may be due to the fact that less of the physiological component is being analyzed. More acquisitions should be done in order to assess what patterns will be observed: namely, if there will continue to be channels where the success rate is 100% and/or if there will be a decrease followed by an increase in hits in the same proportion as observed.

CHAPTER 6

CONCLUSION AND FUTURE WORK

The designed algorithm showed promise in retrieving the m-sequence shown. In all the acquisitions in the test set, the m-sequence with the highest hit rate and also the only one detected was the one previously shown (m-sequence 11). Higher successful retrieval rates were observed in higher cutoff frequencies, which may indicate that most of the signal being analyzed in those conditions did not result from physiological activity but from noise in the FC, as it tends to display a similar behaviour to the one observed when a much higher cutoff frequency is used, i.e., where biological signal is known to be absent.

Building the templates for the estimation using all the segments corresponding to each bit, for each channel, has already been proven to work efficiently. However, in order to reduce computational costs and truly assess the efficiency of the algorithm, fewer segments should be used (4 or 5).

Furthermore, more tests should be run in order to find out why in some channels there was an abnormal 100% hit rate, as it happened to 50% of the acquisitions performed. It should be studied if this was purely circumstantial or if it is an indicator of an interesting pattern. In a way, this event could be explained by considering that some of the electrodes were positioned in places where the signal was not detected as effectively, which led to lower energy in the signal measured belonging to the subject in those places and consequently, less dominance of the physiological component over the noise in the FC.

If, by analyzing more subjects, this high proportion continues to be observed, appropriate corrections should be made. It is worth noting, nonetheless, that this constitutes a first step in order to understand the potential for this algorithm as, if the results hadn't been positive, it would prove as an idea to be abandoned.

In order to further evaluate the potential for this model to discriminate patterns between healthy and unhealthy subjects, more work should be put into addressing the next bullet points:

- evaluate the performance of the software with other sequences in order to increase its degree of confidence;
- test its efficiency with other age groups in order to gauge whether the patterns currently discovered will hold or change;
- compare the results between healthy and unhealthy people in the same age group to assess differences in patterns;
- study and compare the performance in patients diagnosed with more than one disease and possibly, earlier, to either assess the possibility of becoming a precedent to distinguish between diseases and/or find out if there are any pre-diagnostic detection patterns that can serve as an indicator of the presence of pathology for an earlier diagnosis.

BIBLIOGRAPHY

[1] J. M. Lourenço. *The NOVAthesis LaTeX Template User's Manual*. NOVA University Lisbon. 2021. URL: https://github.com/joaomlourenco/novathesis/raw/master/template.pdf (cit. on p. iii).

[2] M. Kayaalp. "Multifaceted Ontological Networks: Methodological Studies toward Formal Knowledge Representation". PhD thesis. 1993-12. DOI: 10.13140/2.1.2902.5928 (cit. on p. 1).

[3] N. Srinivasan. "Cognitive neuroscience of creativity: EEG based approaches". In: *Methods* 42.1 (2007). Neurocognitive Mechanisms of Creativity: A Toolkit, pp. 109–116. ISSN: 1046-2023. DOI: https://doi.org/10.1016/j.ymeth.2006.12.008. URL: https://www.sciencedirect.com/science/article/pii/S1046202306003094 (cit. on p. 2).

[4] G. Alizadeh, T. Y. Rezaii, and S. Meshgini. "Automatic Epileptic Seizure Prediction Based on Convolutional Neural Network and EEG Signal". In: (2023). DOI: 10.20944/PREPRINTS202306.0623.V1. URL: https://www.preprints.org/manuscript/202306.0623/v1 (cit. on p. 2).

[5] Z. S. Khachaturian. "Diagnosis of Alzheimer's Disease". In: *Archives of Neurology* 42 (11 1985-11), pp. 1097–1105. ISSN: 0003-9942. DOI: 10.1001/ARCHNEUR.1985.04060100083029. URL: https://jamanetwork.com/journals/jamaneurology/fullarticle/584730 (cit. on p. 2).

[6] R. T. Rato, L. B. Palma, and A. G. Batista. "Empirical models for horizontal saccadic eye movements". In: *Proceedings - 2014 7th International Conference on Human System Interactions, HSI 2014* (2014), pp. 67–70. DOI: 10.1109/HSI.2014.6860450 (cit. on p. 2).

[7] W. Li et al. "Eye Tracking Methodology for Diagnosing Neurological Diseases: A Survey". In: *Proceedings - 2020 Chinese Automation Congress, CAC 2020*. Institute of Electrical and Electronics Engineers Inc., 2020, pp. 2158–2162. ISBN: 9781728176871. DOI: 10.1109/CAC51589.2020.9326691 (cit. on p. 2).

[8] M. Teplan. "Fundamentals of EEG measurement". In: *Measurement Science Review* 2.Section 2 (2002), pp. 1–11. URL: http://www.edumed.org.br/cursos/neurociencia/MethodsEEGMeasurement.pdf (cit. on pp. 5, 6).

[9] C. Belkhiria and V. Peysakhovich. "Electro-Encephalography and Electro-Oculography in Aeronautics: A Review Over the Last Decade (2010–2020)". In: *Frontiers in Neuroergonomics* 1.December (2020). DOI: 10.3389/fnrgo.2020.606719 (cit. on pp. 5–9).

[10] H. J. Yoon and S. Y. Chung. "EEG-based emotion estimation using Bayesian weighted-log-posterior function and perceptron convergence algorithm". In: *Computers in Biology and Medicine* 43.12 (2013), pp. 2230–2237. ISSN: 00104825. DOI: 10.1016/j.compbiomed.2013.10.017 (cit. on p. 6).

[11] J. Huang. *Overview of Cerebral Function - Neurologic Disorders - Merck Manuals Professional Edition*. 2019. URL: https://www.merckmanuals.com/en-ca/professional/neurologic-disorders/function-and-dysfunction-of-the-cerebral-lobes/overview-of-cerebral-functionhttps://www.merckmanuals.com/professional/neurologic-disorders/function-and-dysfunction-of-the-cerebral-lobes/overview-of-cerebral-function%0Ahttps://www.merckmanuals.com/professional/neurologic-disorders/function-and-dysfunction-of-the-cerebral-lobes/overv (visited on 2023-02-26) (cit. on p. 7).

[12] D. Stein, Harold A., MD, MSC(Ophth), FRCS(C). "Understanding ophthalmic equipment". In: *The Ophthalmic Assistant: A Text for Allied and Associated Ophthalmic Personnel: Ninth Edition*. 2012. Chap. 12, pp. 143–171. ISBN: 9781455710690. DOI: 10.1016/B978-1-4557-1069-0.00009-8. URL: https://www.clinicalkey.com/#!/content/book/3-s2.0-B9780323394772000105 (cit. on p. 7).

[13] J. Malmivuo and R. Plonsey. "The Electric Signals Originating in the Eye". In: *BioelectromagnetismPrinciples and Applications of Bioelectric and Biomagnetic Fields*. Oxford University Press, 1995. Chap. 28. ISBN: 9780195058239. DOI: 10.1093/ACPROF:OSO/9780195058239.001.0001. URL: https://academic.oup.com/book/25966 (cit. on pp. 7, 8).

[14] Terao Y., Fukuda H., and Hikosaka O. "What do eye movements tell us about patients with neurological disorders?" In: *Proceedings of the Japan Academy* 93 (2017), pp. 772–801. URL: https://doi.org/10.2183/pjab.93.049 (cit. on pp. 7–9).

[15] R. Barika and O. Faust. "A review of automated sleep stage scoring". In: *Encyclopedia of Sleep and Circadian Rhythms (Second Edition)*. Ed. by C. A. Kushida. Second Edi. Oxford: Academic Press, 2023, pp. 63–73. ISBN: 978-0-323-91094-1. DOI: https://doi.org/10.1016/B978-0-12-822963-7.00244-9. URL: https://www.sciencedirect.com/science/article/pii/B9780128229637002449 (cit. on p. 8).

[16] "Anatomy of the Human Eye Retina". In: (). URL: https://marvellieyecenter.com/anatomy-human-eye/ (cit. on p. 8).

[17] V. S. Pelak. "Ocular Motility of Aging and Dementia". In: *Current Neurology and Neuroscience Reports* 10.6 (2010), pp. 440–447. ISSN: 1534-6293. DOI: 10.1007/s11910-010-0137-z. URL: https://doi.org/10.1007/s11910-010-0137-z (cit. on p. 8).

[18] A. Bulling et al. "Eye movement analysis for activity recognition using electrooculography". In: *IEEE Transactions on Pattern Analysis and Machine Intelligence* 33.4 (2011), pp. 741–753. ISSN: 01628828. DOI: 10.1109/TPAMI.2010.86 (cit. on pp. 8, 9).

[19] R. J. Leigh and C. Kennard. "Using saccades as a research tool in the clinical neurosciences". In: *Brain* 127.3 (2004), pp. 460–477. ISSN: 00068950. DOI: 10.1093/brain/awh035 (cit. on p. 10).

[20] P. L. Müller and T. Meigen. *M-sequences in ophthalmic electrophysiology.* 2016. DOI: 10.1167/16.1.15. URL: https://pubmed.ncbi.nlm.nih.gov/26818968/ (cit. on pp. 10, 13, 24).

[21] M. Viswanathan. *Wireless Communication Systems in Matlab: Second Edition.* Mathuranathan Viswanathan, 2020, p. 382. ISBN: 9798648350779. URL: https://www.gaussianwaves.com/2018/09/maximum-length-sequences-m-sequences/https://www.gaussianwaves.com/2014/07/power-delay-profile/ (cit. on p. 10).

[22] G. T. Buračas and G. M. Boynton. "Efficient design of event-related fMRI experiments using m-sequences". In: *NeuroImage* 16.3 I (2002), pp. 801–813. ISSN: 10538119. DOI: 10.1006/nimg.2002.1116. URL: https://pubmed.ncbi.nlm.nih.gov/12169264/ (cit. on p. 10).

[23] R. J. McEliece. *Finite Fields for Computer Scientists and Engineers.* Boston, MA, 1993. DOI: 10.1109/TIT.1993.1603956. URL: http://link.springer.com/10.1007/978-1-4613-1983-2 (cit. on pp. 10–12).

[24] Y. Nishitani et al. "Detection of M-sequences from spike sequence in neuronal networks". In: *Computational Intelligence and Neuroscience* 2012 (2012). ISSN: 16875265. DOI: 10.1155/2012/862579. URL: https://pubmed.ncbi.nlm.nih.gov/22851966/ (cit. on pp. 11, 23).

[25] F. Jacobsen. *Fundamentals of General Linear Acoustics.* 2013, p. 300. ISBN: 3715652438. URL: http://eu.wiley.com/WileyCDA/WileyTitle/productCd-1118346416.html (cit. on p. 12).

[26] A. Note. "Manchester Data Encoding for Radio Communications". In: (2005), pp. 1–5. URL: https://www.maximintegrated.com/en/design/technical-documents/app-notes/3/3435.html (cit. on p. 13).

[27] A. S. Tanenbaum and D. J. Wetherall. *Computer Networks: International Version.* Pearson Education, 2010, p. 960. ISBN: 0132553171. URL: http://www.amazon.co.uk/Computer-Networks-International-Andrew-Tanenbaum/dp/0132553171 (cit. on p. 14).

[28] L. Jameel and L. W. Jameel. "Manchester Coding and Decoding Generation Theortical and Expermental Design". In: *American Scientific Research Journal for Engineering* September (2019). ISSN: 2313-4402. URL: http://asrjetsjournal.org/ (cit. on p. 14).

[29] C. E. Shannon. "A Mathematical Theory of Communication". In: *Bell System Technical Journal* 27.3 (1948), pp. 379–423. ISSN: 15387305. DOI: 10.1002/j.1538-7305.1948.tb01338.x (cit. on p. 17).

[30] A. B. Fontaine and W. W. Peterson. "On coding for the binary symmetric channel". In: *Transactions of the American Institute of Electrical Engineers, Part I: Communication and Electronics* 77.5 (2013), pp. 638–647. ISSN: 0097-2452. DOI: 10.1109/tce.1958.6372700 (cit. on p. 17).

[31] S. D. Constantin and T. R. Rao. "On the theory of binary asymmetric error correcting codes". In: *Information and Control* 40.1 (1979), pp. 20–36. ISSN: 00199958. DOI: 10.1016/S0019-9958(79)90329-2 (cit. on pp. 17, 18).

[32] D. J. C. Mackay. *Information Theory, Inference, and Learning Algorithms*. 1995. ISBN: 0521642981. URL: http://www.inference.phy.cam.ac.uk/mackay/itila/ (cit. on p. 18).

[33] J. C. Bancroft. "Introduction to matched filters". In: *CREWES Research Report* 14 (2002), p. 1 (cit. on p. 18).

[34] E. Kabalci and Y. Kabalci. "Cognitive radio based smart grid communications". In: *From Smart Grid to Internet of Energy* (2019-01), pp. 209–248. DOI: 10.1016/B978-0-12-819710-3.00006-5 (cit. on p. 18).

[35] M. Mera-Gaona et al. "Epileptic spikes detector in pediatric EEG based on matched filters and neural networks". In: *Brain Informatics* 7 (1 2020-12), pp. 1–10. ISSN: 21984026. DOI: 10.1186/S40708-020-00106-0/TABLES/6. URL: https://braininformatics.springeropen.com/articles/10.1186/s40708-020-00106-0 (cit. on p. 18).

[36] W. N. Waggener. *Pulse code modulation techniques : with applications in communications and data recording*. Van Nostrand Reinhold, 1995, p. 368. ISBN: 9780442014360. URL: https://link.springer.com/book/9780442014360https://www.booktopia.com.au/pulse-code-modulation-techniques-william-n-waggener/book/9780442014360.html (cit. on p. 18).

[37] G. M. Hatzilabrou et al. "A Comparison of Conventional and Matched Filtering Techniques for Rapid Eye Movement Detection of the Newborn". In: *IEEE Transactions on Biomedical Engineering* 41.10 (1994), pp. 990–995. ISSN: 15582531. DOI: 10.1109/10.324532 (cit. on p. 21).

[38] S. L. Bell, R. Allen, and M. E. Lutman. "The feasibility of maximum length sequences to reduce acquisition time of the middle latency response". In: *The Journal of the Acoustical Society of America* 109.3 (2001), pp. 1073–1081. ISSN: 0001-4966. DOI: 10.1121/1.1340645 (cit. on p. 22).

[39] F. Völk et al. "Measurement of Head Related Impulse Responses for Psychoacoustic Research". In: *Nag/Daga 2009*. 2009, pp. 164–167 (cit. on p. 22).

[40] C. Stamoulis and B. S. Chang. "Application of matched-filtering to extract EEG features and decouple signal contributions from multiple seizure foci in brain malformations". In: *2009 4th International IEEE/EMBS Conference on Neural Engineering, NER '09* (2009), pp. 514–517. DOI: 10.1109/NER.2009.5109346 (cit. on p. 22).

[41] K. Janacsek et al. "Sequence learning in the human brain: A functional neuroanatomical meta-analysis of serial reaction time studies". In: *NeuroImage* 207.May 2019 (2020), p. 116387. ISSN: 10959572. DOI: 10.1016/j.neuroimage.2019.116387. URL: https://doi.org/10.1016/j.neuroimage.2019.116387 (cit. on p. 23).

[42] Q. Yang, M. P. Bucci, and Z. Kapoula. "The latency of saccades, vergence, and combined eye movements in children and in adults". In: *Investigative Ophthalmology and Visual Science* 43.9 (2002), pp. 2939–2949. ISSN: 01460404 (cit. on p. 29).

[43] F. J. Wolters et al. “Coronary heart disease, heart failure, and the risk of dementia: A systematic review and meta-analysis”. In: *Alzheimer's and Dementia* 14.11 (2018), pp. 1493–1504. ISSN: 15525279. DOI: 10.1016/j.jalz.2018.01.007. URL: https://doi.org/10.1016/j.jalz.2018.01.007 (cit. on p. 31).

[44] K. Kasanuki et al. “Impaired heart rate variability in patients with dementia with Lewy bodies: Efficacy of electrocardiogram as a supporting diagnostic marker”. In: *Parkinsonism and Related Disorders* 21.7 (2015), pp. 749–754. ISSN: 18735126. DOI: 10.1016/j.parkreldis.2015.04.024. URL: http://dx.doi.org/10.1016/j.parkreldis.2015.04.024 (cit. on p. 31).

APPENDIX A

EXPERIMENTAL PROTOCOL

A.1 ESPAÇOS

1. Sala 1 (controlo da aquisição)
2. Gaiola de Faraday (aquisição)

A.2 EQUIPAMENTO

1. BioSemi 8A + 8EXG + Bateria (A e B)
2. Gel condutor
3. Cartão para cobrir o ecrã
4. PC de aquisição (sala 1)
5. PC de apresentação dos estímulos (Gaiola de Faraday)
6. Cabo vermelho (com 1 metro de comprimento)
7. T-shirt de laboratório
8. Termo de responsabilidade e matrícula para fotografia do sujeito experimental
9. Guia de disposição dos eléctrodos no sujeito experimental

A.3 CARGOS E RESPONSABILIDADES

- Realizador
  - Organizar e estruturar a experiência;
  - Dirigir os colegas e sujeito experimental;
  - Supervisionar a realização das tarefas;
  - Responsável pelo manuseamento do equipamento;
  - Registo fotográfico.
- Técnico de aquisição
  - Coordena todo o procedimento com o Realizador;
  - Responsável pelo PC de aquisição;
  - Verifica a qualidade dos canais;
  - Verifica o sinal dos fototransístores;
  - Configura, inicia e termina a gravação de dados.
- Técnico experimental
  - Coordena todas o procedimento com o Realizador;
  - Responsável pelo PC de apresentação dos estímulos;
  - Responsável pela montagem do equipamento;
  - Verificar o cumprimento do Doc 2, disponível na Sala 1 e na Gaiola.
- Sujeito Experimental
  - Preencher o Termo de Responsabilidade;
  - Seguir as instruções fornecidas.

Em todos os momentos, o Realizador deve estar presente para assegurar o correto uso dos equipamentos e dos espaços.

A.4 PREPARAÇÃO DA SALA / GAIOLA DE FARADAY

- Sala 1
  1.
  2. Retirar todos os acessórios (mochilas, casacos,...) que possam danificar o equipamento e dificultar a circulação nos espaços;

3. Abrir o armário e retirar as T-shirts de laboratório;
4. Colocar a T-shirt de laboratório;
5. Ligar o PC de aquisição, iniciar sessão no utilizador Mna;
6. Iniciar o software da BioSemi.

- Gaiola de Faraday
  - Verificar todo o equipamento. Reportar caso se verifiquem anormalidades (como as que em seguida se listam), corrigindo antes de prosseguir:
    * PC de apresentação dos estímulos ligado;
    * Mal posicionamento do equipamento;
    * Danos nos eléctrodos;
    * ...

A.5 PREPARAÇÃO DA EXPERIÊNCIA

Interior da Gaiola de Faraday

1. Colocar o PC de estímulos na secretária.
2. Verificar a bateria do PC de estímulos (caso esteja baixa, colocá-lo a carregar).
3. Iniciar sessão no PC de estímulos.
4. Colocar a apresentação de slides com os estímulos visuais que irão ser utilizados durante a experiência.

Exterior da Gaiola de Faraday

1. Criar a pasta que diz respeito à aquisição, com o ReadMe, o Protocolo Detalhado e os slides que irão ser usados na experiência.
2. Preencher o documento 1.Formulário de Aquisição com as informações da mesma, nomeadamente, com as condições de temperatura, humidade, nomes dos técnicos e realizador, etc.
3. Explicar ao sujeito experimental como irá proceder a experiência.
4. Fornecer ao sujeito experimental para preenchimento o documento 2.Termo de responsabilidade, que deve ser impresso e posteriormente arquivado.

Interior da Gaiola de Faraday

1. Sentar o sujeito experimental em frente do PC de apresentação dos estímulos à distância de 1 metro (usar o cabo vermelho à disposição para o efeito).

2. O Técnico de Experiência inicia a colocação dos eléctrodos de EEG da esquerda para direita ou vice-versa e seguindo a disposição que se encontra do documento 3.Disposição eléctrodos EEG EOG *Nota: Os eléctrodos não devem estar ligados ao equipamento.*

3. Após a colocação dos eletrodos de EEG, colocar os eléctrodos de EOG no sujeito experimental. *Os eléctrodos não devem estar ligados ao equipamento.*

4. Ligar todos os eléctrodos ao equipamento.

5. Ligar o equipamento e verificar que a luz azul está acesa, se a bateria ligada se encontra carregada e, em caso negativo, trocá-la.

6. Ligar a fibra ótica.

Exterior da Gaiola de Faraday

1. Verificar no PC de aquisição que a luz azul se encontra ligada.

2. Iniciar o ficheiro para aquisição, desselecionando as opções de pré filtragem, a frequência de amostragem e canais selecionados, e verificando se as impedâncias possuem um valor baixo (< 10 kOhm). *Nota: Caso se verifiquem irregularidades, confirmar a posição e a quantidade de gel no(s) eléctrodos(s) em questão.*.

Interior da Gaiola de Faraday

1. Verificar qual a bateria em utilização.

2. Fazer o registo fotográfico do posicionamento dos eléctrodos e da disposição da sala. Para as fotografias ao sujeito experimental, o registo de matrícula deve ocultar o rosto do sujeito experimental, de forma a ver-se apenas os olhos e a testa. Devem ser tiradas 6 fotografias ou vídeo que inclua:

    - Vista Frontal da face do sujeito experimental;
    - Vista Lateral Direita da face e cabeça do sujeito experimental;
    - Vista Lateral Esquerda da face e cabeça do sujeito experimental;
    - Vista Traseira da cabeça do sujeito experimental;
    - Vista frontal afastada de forma a ver-se os eléctrodos dos pulsos e do rosto;
    - Vista panorâmica da sala.

3. Colocar os foto transístores nos cantos superior esquerdo (fio verde) e inferior direito (fio vermelho), cobrindo-os com o cartão disponível para o efeito.

4. Desligar o quadro elétrico da Gaiola de Faraday.
5. Colocar a sala em ground, ligando a tomada para o efeito.
6. Iniciar a gravação da experiência.
7. Iniciar a apresentação dos slides.
8. Abandonar a Gaiola de Faraday da sala e fechar a porta.

A.6 PREPARAÇÃO DO SUJEITO EXPERIMENTAL

1. Entrar na sala 1.
2. Fornecer uma breve explicação sobre o procedimento da experiência.
3. Dar ao sujeito experimental para responder a declaração de consentimento informado.
4. Entrar na gaiola, após indicação, deixando todos os seus pertences (nomeadamente dispositivos eletrónicos) no exterior da gaiola, e sentar-se na cadeira experimental.

A.7 EXPERIÊNCIA

- A sala deve permanecer em silêncio;
- O Tecnico de Aquisição deve estar atento às transições dos foto transístores e verificar o seu correto funcionamento durante toda a experiência. No caso de este não se verificar, a experiência deve ser interrompida e posteriormente retomada.

1. Após o Técnico de Aquisição verificar que já não se dão mais transições, este reporta ao Realizador que o fim da experiência e termina a gravação do ficheiro.
2. O Técnico de Experiência entra na Gaiola de Faraday e retira a tomada do Ground
3. O Realizador liga o quadro elétrico.

A.8 PÓS EXPERIÊNCIA

1. O Técnico de Aquisição transfere os ficheiros para o Disco Externo e assiste os colegas na Gaiola de Faraday.
2. O Técnico de Experiência desliga o equipamento.
3. O Técnico de Experiência remove os eléctrodos do sujeito experimental e desconecta-os do equipamento.
4. O Técnico de Experiência desconecta o cabo de fibra ótica.

5. O sujeito experimental sai da Gaiola de Faraday após qualquer limpeza que seja necessária. Na Sala 1, recolhe os seus pertences e é dispensado pelo Realizador.

6. Os eléctrodos são limpos, removendo com papel o gel excedente. São posteriormente passados por água da torneira, secos com papel e pendurados no cabide para o efeito, disposto com o mínimo de nós possível.

7. A bateria utilizada é colocada a carregar.

8. Os foto transístores são retirados do ecrã do PC de estímulos.

9. O PC de estímulos é desligado e arrumado.

10. É verificado todo o equipamento e feito um registo fotográfico da disposição final da Gaiola.

11. A Gaiola de Faraday é abandonada e trancada.

A.9 ENCERRAMENTO

1. Todos os participantes despem a T-shirt de laboratório.

2. O Realizador dobra as T-shirts e arruma-as devidamente.

3. É feita a transferência dos dados da aquisição para o disco externo.

4. Desligar o PC de aquisição.

5. Sair e trancar a sala.

6. Colocar as fotografias e um scan do termo de responsabilidade na pasta que diz respeito à Aquisição.

APPENDIX B

DATA SCIENCE PIPELINE

Table B.1: Science Pipeline.

Process / File		X.bdf	X.mat	ku08Green.mat	ku08Red.mat	ku08Green259.mat	ku08Red259.mat	DataXbEx1o16.mat	DataXEx1o16.mat	DataXfEx1o16.mat	SpotLocsUpDwAll.mat	rSegmentsG1ToG16.mat	DifSegments.mat	rMESegmentsG1ToG16t.mat	Sondas.mat	rMSeqs127.mat
BioSemi	Collects the electrical response coming from the scalp (EEG) and the eye area (EOG) and turns it into a .bdf file.	O														
FazAoo BDFto MATLAB	Converts the .bdf file into a .mat file using the EEGLAB toolbox.	I	O													

Table B.1 continued from previous page

Process / File		χ.bdf	χ.mat	ku08Green.mat	ku08Red.mat	ku08Green259.mat	ku08Red259.mat	DataχbExit016.mat	DataχExit016.mat	DataχfExit016.mat	SpotLocsUpDwAll.mat	rSegmentsG1ToG16.mat	AllSegments.mat	rMESegmentsG1ToG16f.mat	Sondas.mat	rMSeqs127.mat
FazA01 Info Transistors	Uses the information in the Status channel to access the state of the photo transistors.	I		O	O											
FazA02 Conta 259Slides	Checks if the number of counted slides is equal to the number of predicted slides.			I	I	O	O									
FazA03 DataX	Produces a file with each channel's information stored in one variable.		I					O								
FazA04 Filtra 50Hz DataNew	Filters the 50 Hz noise coming from the power grid out of the file produced in the previous function.							I	O							
FazA05 Filtra HP05Hz DataNew	High pass filter 0.5 Hz								I	O						
FazA05 Filtra HP2Hz DataNew	High pass filter 2 Hz								I	O						

Table B.1 continued from previous page

Process / File		χ.bdf	χ.mat	ku08Green.mat	ku08Red.mat	ku08Green259.mat	ku08Red259.mat	Dataχbexto16.mat	Dataχexto6.mat	Dataχfexto16.mat	SpotLocsUpDwAll.mat	rSegmentsG1ToG16.mat	AllSegments.mat	rMESegmentsG1ToG16t.mat	Sondas.mat	rMSeqs127.mat
FazA05 Filtra HP10Hz DataNew	High pass filter 10 Hz								I	O						
FazA05 Filtra HP30Hz DataNew	High pass filter 30 Hz								I	O						
FazA06 SpotsLocs	Produces a file with all the locations in number of samples of where the transistors' transistions occured and whether they were up or down transitions.					I					O					
FazA07 Segments	Cuts 350 ms long segments from each channel, each one starting in a moment a down transition occurs in the transistor.									I	I	O				
FazA08 Calcula Diferenciais	It calculates the differential channels' segments.											I	O			

Table B.1 continued from previous page

Process / File		χ.bdf	χ.mat	ku08Green.mat	ku08Red.mat	ku08Green259.mat	ku08Red259.mat	Dataχbex1to16.mat	Dataχex1to6.mat	Dataχfex1to16.mat	SpotLocsUpDwAll.mat	rSegmentsG1ToG16.mat	AllSegments.mat	rMESegmentsG1ToG16t.mat	Sondas.mat	rMSeqs127.mat
FazA09 Normaliza	It normalizes all the segments (unipolar and differential).												I	O		
FazA10 Sondas	It computes the templates for the matched filtering using temporal summation.													I	O	I
FazA11 Detecao	It performs the matched filtering and estimates the m-sequences for each channel, and calculates the number of hits for each channel, relative to each m-sequence of the original set.													I	I	I

ANNEX I

DESIGN OF THE FILTERS USED

I.1 High pass filter with cutoff frequency 0.5 Hz

Table I.1: High pass filter with cutoff frequency 0.5 Hz.

Frequency breakpoints (FB) (Hz)	0	0.2	0.4	0.5	$\frac{f_s}{2}$
Gain	0	0	0.1	1	1

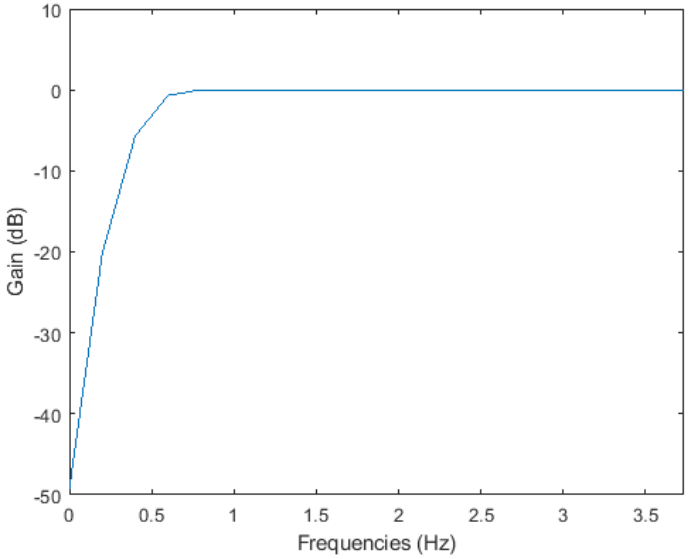

Figure I.1: High pass filter with cutoff frequency 0.5 Hz.

I.2 High pass filter with cutoff frequency 2 Hz

Table I.2: High pass filter with cutoff frequency 2 Hz.

FB (Hz)	0	1	2	$\frac{f_s}{2}$
Gain	0	0.3	1	1

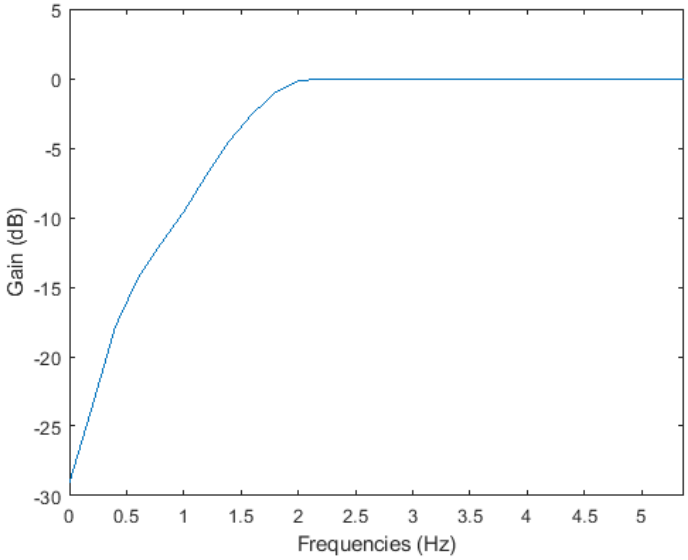

Figure I.2: High pass filter with cutoff frequency 2 Hz.

I.3 High pass filter with cutoff frequency 10 Hz

Table I.3: High pass filter with cutoff frequency 10 Hz.

FB (Hz)	0	7	10	$\frac{f_s}{2}$
Gain	0	0.7	1	1

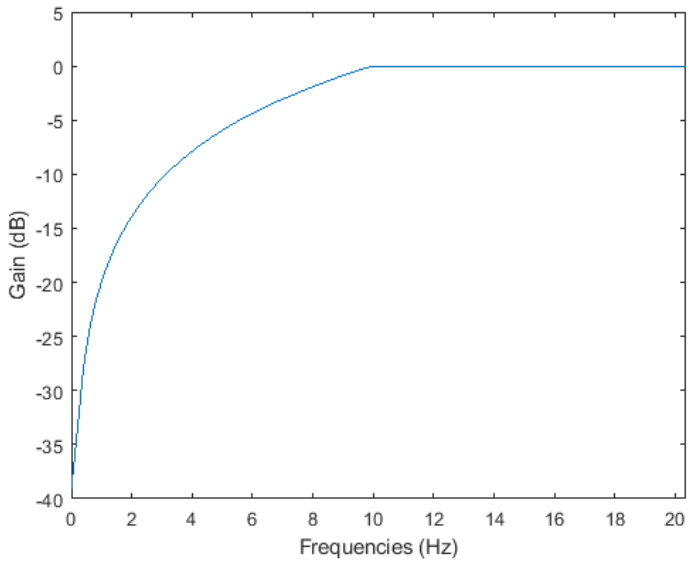

Figure I.3: High pass filter with cutoff frequency 10 Hz.

I.4 High pass filter with cutoff frequency 30 Hz

Table I.4: High pass filter with cutoff frequency 30 Hz.

FB (Hz)	0	10	29	$\frac{f_s}{2}$
Gain	0	0.3	1	1

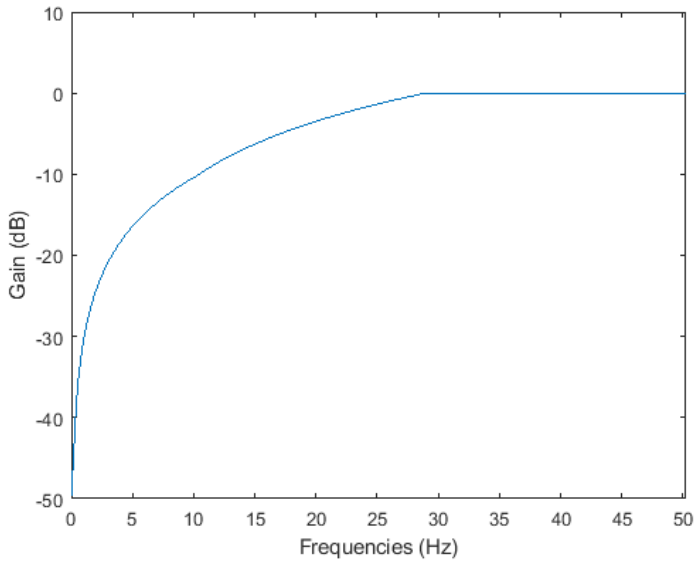

Figure I.4: High pass filter with cutoff frequency 30 Hz.

ANNEX II

RESULTS ANALYSIS

Table II.1: Results for the 0.5 Hz high pass analysis of subject M11FA.

	1	2	3	4	...	9	10	11	12	...	124	125	126	127
HitsA1A2	62	66	70	60	...	68	56	104	66	...	60	60	68	64
HitsA1A3	61	63	71	61	...	59	57	93	67	...	65	65	63	59
HitsA1A4	61	63	69	57	...	69	63	93	69	...	65	63	65	59
HitsA1A5	62	62	70	62	...	66	58	98	70	...	64	68	64	60
HitsA1A6	59	61	69	61	...	65	59	99	67	...	65	65	63	59
HitsA1A7	61	63	67	57	...	63	61	93	67	...	63	67	65	57
HitsA1A8	60	60	70	62	...	64	60	98	62	...	64	66	66	60
HitsA1E1	68	70	60	58	...	68	58	96	62	...	68	70	64	66
HitsA1E2	67	65	63	61	...	69	55	101	63	...	57	59	65	71
HitsA1E3	64	68	58	62	...	66	74	96	60	...	56	58	62	72
HitsA1E4	60	62	68	60	...	74	56	106	66	...	60	62	68	62
HitsA1E5	67	51	71	71	...	61	57	85	69	...	73	57	61	61
HitsA1E6	63	61	67	63	...	67	57	99	63	...	65	59	69	59
HitsA1E7	63	53	71	67	...	67	61	87	63	...	61	63	61	59
HitsA1E8	75	59	69	61	...	69	61	95	63	...	63	61	61	67
HitsA2A3	68	60	64	58	...	66	62	102	60	...	58	54	66	70
HitsA2A4	64	64	60	62	...	66	62	102	64	...	54	58	70	66
HitsA2A5	70	64	60	58	...	66	60	100	58	...	58	58	68	68
HitsA2A6	72	68	66	58	...	66	62	96	60	...	60	58	74	72
HitsA2A7	63	59	63	55	...	71	63	99	63	...	55	59	67	67
HitsA2A8	67	65	63	57	...	71	61	95	65	...	53	63	69	67
HitsA2E1	58	62	66	58	...	68	64	104	64	...	64	60	68	64
HitsA2E2	68	78	54	58	...	62	64	92	56	...	58	66	68	76
HitsA2E3	65	63	67	53	...	67	65	105	63	...	59	59	65	69
HitsA2E4	66	62	70	64	...	66	54	106	60	...	64	64	68	64
HitsA2E5	64	66	64	56	...	68	58	96	56	...	60	62	60	62
HitsA2E6	68	64	62	64	...	68	56	86	72	...	72	62	70	60

Table II.1 continued from previous page

	1	2	3	4	...	9	10	11	12	...	124	125	126	127
HitsA2E7	69	57	65	69	...	61	57	89	61	...	63	63	63	63
HitsA2E8	65	65	69	59	...	55	67	91	61	...	59	59	67	67
HitsA3A4	65	65	67	69	...	59	71	101	71	...	63	61	61	59
HitsA3A5	56	58	62	68	...	60	62	102	68	...	72	64	62	66
HitsA3A6	61	63	67	63	...	63	69	101	61	...	67	63	61	69
HitsA3A7	69	65	69	65	...	63	71	87	55	...	63	67	67	63
HitsA3A8	62	54	66	64	...	60	72	96	62	...	68	64	68	64
HitsA3E1	57	65	67	59	...	63	59	89	69	...	65	67	63	69
HitsA3E2	63	69	57	63	...	63	65	97	63	...	53	61	67	67
HitsA3E3	60	64	70	58	...	68	64	98	62	...	64	66	66	64
HitsA3E4	66	56	64	62	...	66	64	112	62	...	58	58	64	64
HitsA3E5	67	71	69	63	...	65	57	87	61	...	65	67	59	65
HitsA3E6	66	64	60	64	...	68	66	98	66	...	62	58	72	60
HitsA3E7	66	58	64	70	...	64	56	90	60	...	64	62	62	60
HitsA3E8	75	63	71	63	...	63	63	91	55	...	59	67	59	71
HitsA4A5	61	59	69	63	...	59	57	95	69	...	63	69	63	69
HitsA4A6	65	55	69	61	...	61	63	93	69	...	63	65	67	69
HitsA4A7	65	65	67	63	...	63	71	89	61	...	59	65	69	67
HitsA4A8	64	54	60	60	...	56	62	96	60	...	64	66	72	66
HitsA4E1	61	71	69	59	...	67	65	87	65	...	67	65	63	65
HitsA4E2	65	69	59	65	...	65	61	99	65	...	59	61	69	67
HitsA4E3	60	64	66	60	...	68	64	98	64	...	62	60	64	66
HitsA4E4	62	60	64	64	...	68	62	106	66	...	54	62	68	68
HitsA4E5	68	72	66	66	...	70	62	88	60	...	60	62	62	68
HitsA4E6	63	61	61	63	...	67	61	97	63	...	59	63	73	61
HitsA4E7	66	58	64	74	...	66	54	88	58	...	60	62	62	64
HitsA4E8	75	63	73	61	...	65	61	91	55	...	57	67	63	73
HitsA5A6	70	58	66	58	...	64	68	104	68	...	68	60	64	60
HitsA5A7	70	70	64	60	...	66	50	88	68	...	64	62	58	68
HitsA5A8	65	65	67	55	...	57	65	103	59	...	71	57	73	59
HitsA5E1	60	62	68	54	...	70	60	90	72	...	66	68	62	64
HitsA5E2	69	69	57	61	...	63	59	95	59	...	53	65	69	65
HitsA5E3	63	67	69	57	...	67	63	105	69	...	63	65	61	63
HitsA5E4	67	57	61	61	...	65	59	107	59	...	57	61	67	67
HitsA5E5	69	69	67	57	...	67	67	89	67	...	63	65	65	67
HitsA5E6	65	61	59	63	...	67	63	97	65	...	61	59	75	61
HitsA5E7	70	56	60	66	...	62	56	88	62	...	66	62	64	60
HitsA5E8	68	70	68	60	...	64	66	88	64	...	64	62	60	70
HitsA6A7	66	64	62	66	...	64	62	88	72	...	66	64	62	64
HitsA6A8	70	70	62	56	...	56	56	96	54	...	68	64	68	68
HitsA6E1	56	62	68	56	...	66	64	94	66	...	62	64	62	60
HitsA6E2	68	72	62	60	...	64	60	90	56	...	58	64	68	70
HitsA6E3	64	62	66	54	...	66	68	100	68	...	62	62	60	64
HitsA6E4	63	57	65	63	...	69	63	107	61	...	55	59	69	69
HitsA6E5	59	67	65	59	...	69	65	95	65	...	63	65	65	63
HitsA6E6	64	64	56	64	...	72	64	96	64	...	60	60	72	60

Table II.1 continued from previous page

	1	2	3	4	...	9	10	11	12	...	124	125	126	127
HitsA6E7	71	55	63	69	...	61	57	89	63	...	63	63	63	63
HitsA6E8	66	68	66	64	...	64	66	88	62	...	62	60	62	68
HitsA7A8	62	52	66	68	...	66	64	90	68	...	66	68	70	64
HitsA7E1	56	68	70	60	...	66	62	88	62	...	64	62	70	64
HitsA7E2	65	67	59	59	...	65	59	95	63	...	57	61	67	63
HitsA7E3	72	64	64	58	...	64	68	96	62	...	62	66	62	66
HitsA7E4	62	56	64	66	...	68	62	106	64	...	54	58	68	68
HitsA7E5	67	67	65	61	...	63	63	89	65	...	61	63	59	65
HitsA7E6	62	60	62	62	...	70	60	98	66	...	60	62	72	58
HitsA7E7	69	57	65	71	...	63	55	87	61	...	63	63	63	63
HitsA7E8	69	71	65	63	...	63	61	91	61	...	63	65	63	65
HitsA8E1	61	61	71	61	...	61	65	95	65	...	67	69	69	63
HitsA8E2	62	66	62	58	...	68	60	92	60	...	50	62	66	66
HitsA8E3	68	60	70	60	...	64	68	102	60	...	66	68	64	62
HitsA8E4	62	58	62	62	...	70	62	106	66	...	52	60	68	64
HitsA8E5	63	63	63	59	...	65	65	97	61	...	63	67	67	59
HitsA8E6	62	66	60	62	...	70	66	96	66	...	58	60	72	62
HitsA8E7	73	53	63	67	...	63	55	89	61	...	63	65	61	63
HitsA8E8	68	68	68	64	...	64	68	88	60	...	62	62	62	70
HitsAG1	61	73	59	61	...	61	61	95	57	...	67	57	69	63
HitsAG2	60	62	64	64	...	68	70	104	64	...	64	58	72	62
HitsAG3	63	63	55	65	...	55	71	91	61	...	55	59	63	63
HitsAG4	71	63	55	55	...	53	65	85	61	...	61	65	69	65
HitsAG5	67	57	73	57	...	57	63	91	63	...	71	59	69	69
HitsAG6	58	58	70	58	...	60	60	88	68	...	66	58	74	74
HitsAG7	61	53	73	59	...	57	61	85	63	...	65	61	69	65
HitsAG8	61	53	73	67	...	61	65	85	63	...	69	65	73	65
HitsE1E2	57	65	69	59	...	73	57	105	59	...	57	61	69	69
HitsE1E3	63	69	57	59	...	65	63	99	57	...	51	63	61	69
HitsE1E4	61	61	69	59	...	71	63	111	65	...	61	61	69	61
HitsE1E5	72	70	60	66	...	64	58	96	58	...	68	58	60	66
HitsE1E6	58	62	66	62	...	70	62	98	66	...	66	58	70	58
HitsE1E7	66	56	66	68	...	66	60	86	60	...	66	60	58	64
HitsE1E8	74	56	72	62	...	64	62	94	60	...	60	60	62	66
HitsE2E3	62	68	60	56	...	70	60	104	64	...	56	64	66	66
HitsE2E4	60	60	68	62	...	68	64	108	62	...	64	60	68	60
HitsE2E5	66	68	62	62	...	66	56	94	54	...	60	62	64	66
HitsE2E6	69	61	61	73	...	65	57	81	77	...	73	57	61	53
HitsE2E7	69	57	67	69	...	57	57	87	61	...	63	61	65	63
HitsE2E8	59	67	67	63	...	57	65	93	65	...	61	65	65	69
HitsE3E4	59	59	69	57	...	73	61	107	63	...	57	59	67	65
HitsE3E5	58	64	66	66	...	68	70	96	68	...	58	60	70	64
HitsE3E6	62	58	70	60	...	70	62	106	64	...	62	62	66	62
HitsE3E7	64	54	68	66	...	66	60	90	64	...	62	64	62	56
HitsE3E8	75	59	65	59	...	67	67	97	63	...	61	55	63	69
HitsE4E5	67	63	65	57	...	69	61	107	63	...	63	65	57	67

Table II.1 continued from previous page

	1	2	3	4	...	9	10	11	12	...	124	125	126	127
HitsE4E6	64	66	68	64	...	66	60	98	54	...	54	56	62	72
HitsE4E7	66	60	62	60	...	60	62	92	58	...	64	62	64	66
HitsE4E8	57	69	65	67	...	59	59	99	65	...	61	69	69	61
HitsE5E6	63	63	63	61	...	71	63	111	65	...	59	63	67	59
HitsE5E7	66	52	68	64	...	64	62	86	62	...	62	62	64	60
HitsE5E8	74	60	68	64	...	66	60	92	60	...	58	58	60	68
HitsE6E7	69	57	65	65	...	59	59	91	59	...	63	59	67	63
HitsE6E8	51	65	69	67	...	59	65	93	75	...	67	67	69	65
HitsE7E8	64	60	62	66	...	64	56	94	54	...	66	64	56	62
HitsEX1	60	66	62	62	...	66	52	104	60	...	66	66	68	68
HitsEX2	59	67	65	57	...	75	63	101	61	...	57	59	67	69
HitsEX3	62	68	56	58	...	68	62	98	60	...	54	62	64	68
HitsEX4	62	62	70	60	...	70	66	110	68	...	60	60	68	64
HitsEX5	69	71	61	59	...	65	55	93	55	...	59	61	63	65
HitsEX6	60	64	64	64	...	70	66	98	74	...	62	62	62	58
HitsEX7	68	56	64	68	...	64	60	88	60	...	64	60	60	64
HitsEX8	73	67	73	69	...	61	63	93	61	...	57	63	61	71

Table II.1 shows the results obtained for the number of hits when comparing the m-sequence estimated for each channel and each m-sequence in the original set. In the header, are each sequence in the original set, and in the first column, each channel analyzed.